Title
GPS/ INS Based Lateral And Longitudinal Control Demonstration: Final Report

Authors
Farrell, Jay
Barth, Matthew
Galijan, Randy
et al.

Publication Date
1998-08-01

CALIFORNIA PATH PROGRAM
INSTITUTE OF TRANSPORTATION STUDIES
UNIVERSITY OF CALIFORNIA, BERKELEY

GPS/INS Based Lateral and Longitudinal Control Demonstration: Final Report

Jay Farrell, Matthew Barth, Randy Galijan, Jim Sinko

California PATH Research Report
UCB-ITS-PRR-98-28

This work was performed as part of the California PATH Program of the University of California, in cooperation with the State of California Business, Transportation, and Housing Agency, Department of Transportation; and the United States Department of Transportation, Federal Highway Administration.

Report for MOU 292

August 1998

ISSN 1055-1425

CALIFORNIA PARTNERS FOR ADVANCED TRANSIT AND HIGHWAYS

GPS/INS Based Lateral and Longitudinal Control Demonstration
Final Report

Principal Investigator: Jay Farrell
Department of Electrical Engineering
University of California, Riverside
jay.farrell@ucr.edu

Co-Principal Investigator: Matthew Barth
Center for Environmental Research and Technology
University of California, Riverside
barth@cert.ucr.edu

Co-Principal Investigator: Randy Galijan
Stanford Research Institute
Menlo Park, CA
randy_galijan@qm.sri.com

Co-Principal Investigator: Jim Sinko
Stanford Research Institute
Menlo Park, CA
jim_sinko@sdd.sri.com

July 31, 1998

Abstract

This report describes the results of a one year effort to implement and analyze the performance of a Differential Global Positioning System (DGPS) aided Inertial Navigation System (INS) for possible future use in Advanced Vehicle Control Systems (AVCS).

The initial premise of this project was that DGPS/INS technology has the potential to serve as a centimeter-level position reference system as necessary for automated driving functions. Key advantages of this approach include: 1) no changes to the highway infrastructure are required; therefore, the DGPS/INS system should be less expensive to install and maintain than alternative reference systems; 2) knowledge of the DGPS position of a vehicle allows the use of significantly more path preview information than alternative position reference systems; therefore, control performance could be improved; 3) the navigation system would output the full vehicle state (position, velocity, and attitude) and inertial measurements at significantly higher rates than alternative navigation systems would provide even a subset of the vehicle state.

The overall objective of this study was to implement a DGPS aided INS system and to analyze the technical feasibility of such a system relative to the requirements for vehicle control. The one year effort incorporated two main tasks: 1) Implementation of a real-time DGPS/INS; and, 2) Experimental analysis of the DGPS/INS performance. The DGPS/INS system provided estimates of vehicle position, linear velocities, and angular rates. State estimates are currently available at a rate of 100 Hertz, but significantly higher rates are feasible. Position accuracy at the centimeter level is achieved and demonstrated via two experiments. Integration of the DGPS aided INS into a control algorithm was not included in this one year study, but is one of the items discussed under future work.

A few potential follow-on projects include: implementation of the DGPS/INS system in a control demonstration, development and demonstration of more advanced (higher rates and increased accuracy) DGPS/INS systems, analysis of DGPS/INS systems with other sensor systems to achieve required system level reliability specifications, analysis of DGPS/INS AVCS protocols, and analysis of the need and performance of pseudolites in AHS systems. Specific detail regarding such efforts is included in the report conclusions.

Keywords: Global Positioning System, Inertial Navigation, Differential Carrier Phase, Advanced Vehicle Control

Executive Summary

This project was a one year effort to implement and analyze the performance of a Differential Global Positioning System (DGPS) aided Inertial Navigation System (INS) for possible future use in Advanced Vehicle Control Systems (AVCS).

The initial premise of this project was that DGPS/INS technology has the potential to serve as a centimeter-level position reference system as necessary for automated driving functions. Key advantages of this approach include:

1. no changes to the highway infrastructure are required; therefore, the DGPS/INS system should be less expensive to install and maintain than alternative reference systems;
2. knowledge of the DGPS position of a vehicle allows the use of significantly more path preview information than alternative position reference systems; therefore, control performance could be improved;
3. the navigation system would output the full vehicle state (position, velocity, and attitude) and inertial measurements (accelerations and angular rates) at significantly higher rates than alternative navigation systems would provide even a subset of the vehicle state.

The overall objective of this study was to implement a DGPS aided INS system and to analyze the technical feasibility of such a system relative to the requirements for vehicle control. The one year effort incorporated two main tasks:

1. Implementation of a real-time DGPS/INS,
2. Experimental analysis of the DGPS/INS performance.

The DGPS/INS system provided estimates of vehicle position, linear velocities, and angular rates. State estimates are currently available at a rate of 100 Hertz, but significantly higher rates are feasible. Position accuracy at the centimeter level is achieved and demonstrated via two experiments. Integration of the DGPS aided INS into a control algorithm was not included in this one year study, but is one of the items discussed under future work.

A few potential follow-on projects include:

1. implementation of the DGPS/INS system in a control demonstration,
2. development and demonstration of more advanced (higher rates and increased accuracy) DGPS/INS systems
3. analysis of DGPS/INS systems with other sensor systems to achieve required system level reliability specifications
4. analysis of DGPS/INS AVCS protocols, and
5. analysis of the need and performance of pseudolites in AHS systems.

Specific details regarding such efforts are included in the report conclusions.

Contents

Chapter 1

Project Introduction

Automated vehicle position control systems for an AHS require both a means for determining vehicle position and a means for controlling the vehicle position [38, 16]. The vehicle position may be determined in either relative (e.g., position relative to nearby known point) or absolute (e.g., latitude, longitude, altitude) coordinates. A vehicle control system is then designed to maneuver the vehicle along a specified trajectory in the specified coordinate system. A variety of reference positioning systems may be considered: embedded wires [16, 9, 17], embedded magnets [38, 43], radar [16, 31], vision [26, 19, 10, 11, 30, 37, 40], and DGPS technology. This effort has focused on research to develop, analyze, and demonstrate a DGPS aided INS with accuracy and sample rates sufficient for vehicle control.

1.1 Global Positioning System and Vehicle Control

The Global Positioning System [1] is a convenient and accurate method for determining vehicle position in a global coordinate system. The system is built around a constellation of 24 satellites already orbiting the earth. The orbits are designed in a manner that allows the signals from at least four satellites to be received simultaneously at any point on the surface of the earth with an unobstructed via of the sky. Each satellite broadcasts data allowing a user receiver to calculate the satellite (x,y,z) position and user to satellite range. A GPS receiver can use four sets of these signals to determine its own (x,y,z) position (see Section 3.2). GPS navigation systems are currently used in many applications including aircraft [32] and ships [36].

The standard accuracy of GPS position estimates is on the order of 50 meters. Increased accuracy (at the meter level) can be achieved through the use of Differential GPS (DGPS) [32, 25, 42, 4, 5, 12, 15]. Furthermore, a DGPS system that uses carrier phase observations can provide accuracies of 1 to 3 cm. Appropriate techniques are discussed in the Methodology Section of this report.

For vehicle control, a trajectory corresponding to the desired path (i.e., the automated highway lane trajectory) would be defined in the global coordinate reference frame and stored on-board the vehicle. Additional information such as the road inclination, turning radius and direction, and super-elevation angle could also be stored on-board (using CD technology) as a function of roadway position to improve control performance. The vehicle control system would then drive the steering and propulsion actuation systems to force the vehicle to follow the desired trajectory.

Advantages of working with an absolute or global coordinate system are:

1. both lateral and longitudinal position information relative to the desired trajectory are known at all times;
2. the vehicle can always return to the desired path since it always knows its position and the desired position;
3. significant amounts of path preview information can be used to facilitate control;
4. the vehicle velocity profile as a function of global position can be specified; and
5. the global position of the vehicle is available for other purposes (e.g., traveler information, traffic management).

Additional advantages of using the Navstar Global Positioning System include

1. no changes are required to the roadway infrastructure;
2. DGPS can determine 3-dimensional vehicle attitude; and
3. DGPS signals are available in all weather conditions.

The main drawback of a DGPS system is that the satellite signals can be blocked by obstacles (trees, tunnels, buildings). This drawback can be effectively addressed via inertial navigation systems (see below) and pseudolites. See Section 3.2 for a detailed discussion of GPS methods.

1.2 Inertial Navigation and Vehicle Control

For control purposes, it is desirable to know the position and additional vehicle state and inertial information (i.e., position, attitude, velocity, angular rates, linear acceleration) at high (≥ 100 Hz) sampling rates. Inertial Navigation Systems (INS) [6, 7, 14] have been developed and are used in air, land, and sea applications. Such systems are capable of providing the full vehicle state information at rates suitable for accurate vehicle control, even in applications where some of the sensors are sampled at slower rates. A typical INS system integrates the differential equation describing the system kinematics for a short period of time using high rate data from a set of inertial instruments. During this integration process, the error variance of the navigation state increases primarily due to sensor noise and errors in sensor calibration and alignment. After a period of integration, aiding sensor measurements (e.g., GPS) can be used to correct the state estimates. The main advantages of INS systems are:

1. full vehicle state estimates are produced without differentiation (i.e., low sensitivity to high frequency noise);
2. the update rate of the navigation state estimates are not limited by the update rates of the aiding sensors; and
3. the accuracy of the navigation state is not affected by variables or fields external to the navigation system.

The main disadvantage of an unaided INS system is unbounded growth in the position estimation error of the vehicle; however, an INS system used in conjunction with aiding sensors can provide the full state estimates at the desired control frequency more accurately than either technique used individually. In addition, the INS would continue to provide position estimates at times when signals from the position sensing system were not available.

1.3 Redundant Positioning Systems

Taken independently, any positioning system of interest has advantages and disadvantages. The strongest criticism of any of the individual techniques is that it is susceptible to a single point failure. However, used jointly (with effective sensor fusion and fault detection techniques) the overall performance and reliability of the system could be significantly improved. No single reference system can supply adequate reliability and availability to ensure safe longitudinal and lateral control. For example, the requirements for instrument landing systems (ILS) is that the probability of undetected guidance error be less than 3.3×10^{-9} per landing for the entire system, ground and airborne [35]. While todays highway safety could be enhanced with a lower reliability level (Interstate highways have a fatal accident every 2.4×10^6 hours of driving and an injury accident every 58,000 hours), there are political and legal considerations that will push the guidance portions of AHS towards a comparable level of reliability. As in aviation, there will be more tolerance for accidents resulting from human errors and mechanical problems than for accidents resulting from guidance or computer software errors. Since no single black box is likely to have a reliability/availability of better than 0.9999, we can expect that at least two and likely three reference systems will be required. Thus DGPS needs to be seriously considered along with the other referencing systems if three viable independent systems are to be available for AHS.

Consider, for example, a system incorporating an embedded magnet reference system (EMRS), DGPS positioning, and an Inertial Navigation System (INS). A desired path would be specified in global coordinates to pass through the locations of the embedded markers that specify an automated lane1. The INS would provide estimates of state and position relative to the desired trajectory at a rate high enough to satisfy control system requirements, even though the EMRS and GPS measurements occurred at a slower rate. While near the desired trajectory, the three available redundant estimates of vehicle position relative to the desired path would allow effective fault detection and isolation. When the vehicle was significantly off the desired trajectory (e.g., lane changing, entering/leaving a platoon, initialization, disturbances), where the EMRS losses accuracy, the DGPS and INS systems would still provide the accurate position information necessary to complete the maneuver of interest. In addition, knowledge of global vehicle position would facilitate both the process of negotiating maneuvers with neighboring vehicles and the process of determining relative vehicle position and velocity.

Chapter 2

Project Scope and Objectives

Vehicle control based on some form of absolute or global sensing techniques, such as the use of GPS-based sensing, has advantages over relative or local sensing techniques. Used in a complementary fashion, local and global positioning techniques would have substantial reliability and system performance benefits over either positioning system when used independently. However, to date, very little work has been done to harvest the potential utility of global positioning techniques. Technical reasons against the use of the GPS system include 1) the low sampling rates of previously available receivers[1], and 2) the possibility of satellite occlusion which could temporarily eliminate the availability of position estimates. In this project, unique advanced GPS techniques in conjunction with an inertial navigation system have been used to overcome these technical shortcomings.

2.1 Project Objectives

Based on the ideas discussed above, our ultimate objective is to develop and demonstrate an automobile driving autonomously on the DGPS/INS portion of such a navigation system. The immediate objectives for this current one year project are to demonstrate that DGPS/INS systems can ultimately achieve the accuracy and update specifications required for AHS applications. The motivations for pursuing DGPS/INS alone at this time are: 1) to prove the feasibility of the concept; 2) to simplify test and evaluation, as the DGPS/INS demonstration alone can be accomplished at many locations.

2.2 Project Scope

The INS and GPS systems for this effort were collaboratively developed by UCR and SRI. The INS, data acquisition system, and GPS processing software were developed at UCR. SRI provided technical expertise related to carrier phase integer ambiguity resolution. Implementing the DGPS/INS system required the following hardware: two GPS receivers, an INS sensor package, a datalink between a fixed receiver and the mobile receiver on the vehicle, a computer with data acquisition equipment, and ancillary equipment.

[1] Receivers are currently available with raw data output rates above 10 Hz.

Two Ashtech Z-12 GPS receivers, an INS sensor suite, a radio modem system, and two IBM486 compatible personal computers were be supplied by UCR.

Two advanced carrier phase DGPS technologies–carrier smoothing of code measurements and carrier double differencing– were originally proposed for investigation. Using carrier data to smooth code measurements could have resulted in per sample position estimation accuracies of approximately 50 cm (horizontal RMS). Double differencing the offset between the code and carrier measurements to arrive at an average offset would have the potential to improve location accuracies, with 10 cm accuracies seen as possible.

Based on initial analysis, an alternative set of GPS techniques were selected and implemented. The overall approach is defined in Section 3.2. The alternative approach was defined to increase accuracy, reliability, and compatibility with real-time operation.

This project used an existing INS system previously developed at UCR. The scope of the project required the INS system to be modified to include GPS carrier phase aiding, and required experimental analysis of the system performance. The scope of the project did not allow extensive theoretical analysis of system performance in various operating scenarios, advancement of the INS implementation, or vehicle control. Further research in these directions is discussed herein.

Chapter 3

Methodology

The navigation system developed for this project incorporates a strapdown inertial navigation system with various modes of GPS aiding. The following sections discuss each component of the system design. Section 3.1 discusses the INS implementation and error equations. Section 3.2 discusses various issues related to obtaining high accuracy position information from the GPS system. Section 3.3 discusses the use of GPS as an INS aid. Section 3.4 specifies the remainder of the overall system design.

3.1 Inertial Navigation System (INS)

This section summarizes the mechanization equations for a strapdown tangent plane INS. The derivations using the same notation can be found in [14]. The mechanization equations are the computer solution of the INS differential equations based on computed and measured variables. These equations are summarized below, in the Britting notation [6], where $\hat{x}$ and $\tilde{x}$ denote respectively, the computed and measured values of the variable x.

3.1.1 Tangent Plane Mechanization Equations

The (local fixed) tangent plane INS mechanization differential equations are

$$\begin{bmatrix} \dot{\hat{n}} \\ \dot{\hat{e}} \\ \dot{\hat{h}} \\ \dot{\hat{v}}_N \\ \dot{\hat{v}}_E \\ \dot{\hat{v}}_D \end{bmatrix} = \begin{bmatrix} 1 & 0 & 0 \\ 0 & 1 & 0 \\ 0 & 0 & -1 \\ 0 & -2\omega_{ie}\sin(\hat{\lambda}) & 0 \\ 2\omega_{ie}\sin(\hat{\lambda}) & 0 & 2\omega_{ie}\cos(\hat{\lambda}) \\ 0 & -2\omega_{ie}\cos(\hat{\lambda}) & 0 \end{bmatrix} \begin{bmatrix} \hat{v}_N \\ \hat{v}_E \\ \hat{v}_D \end{bmatrix} + \begin{bmatrix} 0 \\ 0 \\ 0 \\ \hat{f}_N \\ \hat{f}_E \\ \hat{f}_D \end{bmatrix} + \begin{bmatrix} 0 \\ 0 \\ 0 \\ 0 \\ 0 \\ \hat{g} \end{bmatrix} \tag{3.1}$$

where all variables are defined in Appendix A. For use in the above equation, the accelerometer measurements are processed as follows:

$$\begin{bmatrix} \hat{f}_N \\ \hat{f}_E \\ \hat{f}_D \end{bmatrix} = \hat{C}_p^n \left(\begin{bmatrix} \tilde{f}_u \\ \tilde{f}_v \\ \tilde{f}_w \end{bmatrix} - \begin{bmatrix} \hat{b}_u \\ \hat{b}_v \\ \hat{b}_w \end{bmatrix} \right).$$

The platform to navigation frame vector transformation matrix is calculated based on the Euler roll, pitch, and yaw angles. The Euler angles are maintained by solving the following differential equations

$$\begin{bmatrix} \dot{\hat{\phi}} \\ \dot{\hat{\theta}} \\ \dot{\hat{\psi}} \end{bmatrix} = \begin{bmatrix} 1 & \sin(\hat{\phi})\tan(\hat{\theta}) & \cos(\hat{\phi})\tan(\hat{\theta}) \\ 0 & \cos(\hat{\phi}) & -\sin(\hat{\phi}) \\ 0 & \frac{\sin(\hat{\phi})}{\cos(\hat{\theta})} & \frac{\cos(\hat{\phi})}{\cos(\hat{\theta})} \end{bmatrix} \begin{bmatrix} \hat{p} \\ \hat{q} \\ \hat{r} \end{bmatrix} \tag{3.2}$$

with the gyro attitude rate measurements as inputs. For use in the above equation, the gyro measurements are processed as follows:

$$\begin{bmatrix} \hat{p} \\ \hat{q} \\ \hat{r} \end{bmatrix} = \left(\begin{bmatrix} \tilde{p} \\ \tilde{q} \\ \tilde{r} \end{bmatrix} - \begin{bmatrix} \hat{b}_p \\ \hat{b}_q \\ \hat{b}_r \end{bmatrix} \right) - \hat{\mathbf{R}}_{n2p} \left(\omega_{ie} \begin{bmatrix} \cos(\hat{\lambda}) \\ 0 \\ -\sin(\hat{\lambda}) \end{bmatrix} \right) \tag{3.3}$$

A quaternion approach would have been preferred, and would be pursued in future efforts, but was not achievable within the given resource constraints. The quaternion approach would have the advantages of faster computation and no singularities. The approach which used here (eqn. (3.2)) achieved the desired update rates and was not affected by the singularities due to the small tilt angles.

The local, fixed tangent plane INS was sufficient for this demonstration due to the limit geographic area expected for testing. In the ultimate application, the geographic INS described in [14] would be required to allow unrestricted (global) travel. Minor changes to the INS are required to transform the currently implemented INS to the geographic (latitude, longitude based) INS.

3.1.2 Tangent Plane INS Nominal Error Equations

For error analysis and on-line error estimation via Kalman filtering (see Section 3.3), it is convenient to linearize the equations of the previous section about the vehicle trajectory. The linearized error equations are derived in [6, 14, 41] and summarized in this and the following subsections. The summary uses the following notation

$$\omega_N = \omega_e \cos(\lambda) \tag{3.4}$$

$$\omega_D = -\omega_e \sin(\lambda) \tag{3.5}$$

for the north and vertical components of earth rotation rate in the navigation frame

The dynamic equations for the linearized INS error are

$$\delta\mathbf{x}(t) = \mathbf{F}(t)\delta\mathbf{x}(t) + \epsilon(t) + \omega(t). \tag{3.6}$$

where

$$\mathbf{F} = \begin{bmatrix} 0 & 0 & 0 & 1 & 0 & 0 & 0 & 0 & 0 \\ 0 & 0 & 0 & 0 & 1 & 0 & 0 & 0 & 0 \\ 0 & 0 & 0 & 0 & 0 & -1 & 0 & 0 & 0 \\ \frac{-2\omega_n v_E}{R} & 0 & 0 & 0 & 2\omega_D & 0 & 0 & f_D & -f_E \\ \frac{2}{R}(v_N\omega_N + v_D\omega_D) & 0 & 0 & -2\omega_D & 0 & 2\omega_N & -f_D & 0 & f_N \\ \frac{-2v_E\omega_D}{R} & 0 & \frac{-2\mu}{R^3} & 0 & -2\omega_N & 0 & f_E & -f_N & 0 \\ \frac{\omega_D}{R} & 0 & 0 & 0 & 0 & 0 & 0 & \omega_D & -\omega_E \\ 0 & 0 & 0 & 0 & 0 & 0 & -\omega_D & 0 & \omega_N \\ \frac{-\omega_N}{R} & 0 & 0 & 0 & 0 & 0 & \omega_E & -\omega_N & 0 \end{bmatrix}. \tag{3.7}$$

Due to the small magnitude of the velocity relative to $\frac{\omega_e}{R}$, the first column can be approximated as zero.

For notational convenience in the following sections, the linearized error equations can be written as

$$\begin{bmatrix} \delta\dot{\mathbf{p}} \\ \delta\dot{\mathbf{v}} \\ \delta\dot{\rho} \end{bmatrix} = \begin{bmatrix} \mathbf{F_{pp}} & \mathbf{F_{pv}} & \mathbf{F_{p\rho}} \\ \mathbf{F_{vp}} & \mathbf{F_{vv}} & \mathbf{F_{v\rho}} \\ \mathbf{F_{\rho p}} & \mathbf{F_{\rho v}} & \mathbf{F_{\rho\rho}} \end{bmatrix} \begin{bmatrix} \delta\mathbf{p} \\ \delta\mathbf{v} \\ \delta\rho \end{bmatrix} + \begin{bmatrix} e_{\mathbf{p}} \\ e_{\mathbf{v}} \\ e_{\rho} \end{bmatrix} + \begin{bmatrix} \omega_{\mathbf{p}} \\ \omega_{\mathbf{v}} \\ \omega_{\rho} \end{bmatrix}. \tag{3.8}$$

The subcomponents of the $\mathbf{F}$ matrix can be defined by inspection of eqn. (3.7). All error quantities are defined to be the actual value minus the calculated (or measured) quantity (i.e., $\delta x = x - \hat{x}$).

For the tangent plane implementation, the three components of nominal error state are defined to be

$$\delta\mathbf{p} = [\delta n, \delta e, \delta h]^T \tag{3.9}$$

$$\delta\mathbf{v}^n = [\delta v_N, \delta v_E, \delta v_D]^T \tag{3.10}$$

$$\delta\rho^n = [\delta\epsilon_N, \delta\epsilon_E, \delta\epsilon_D]^T. \tag{3.11}$$

The error state vector is defined as

$$\delta\mathbf{x}(t) = [\delta\mathbf{p}, \delta\mathbf{v}^n, \delta\rho^n].$$

Instrument and gravity modeling errors are represented by the three subvectors of $\epsilon(t)$.

Equation (3.8) shows that the velocity error is driven by accelerometer and gravitational model errors denoted by $\mathbf{e_v}$. Let $\mathbf{x}_a$ denote the state to be augmented to account for the accelerometer and gravitation errors. Equation (3.8) also shows that the attitude error is driven by gyro errors denoted by $\mathbf{e}_\rho$. Let $\mathbf{x}_g$ denote the state to be augmented to account for these gyro errors. Linear error models can be defined [14] with matrices $\mathbf{F_{v x}}_a$ and $\mathbf{F}_{\rho \mathbf{x}_g}$ such that

$$\mathbf{e_v} = \mathbf{F_{v x}}_a \mathbf{x}_a + \nu_a \tag{3.12}$$

$$\mathbf{e}_\rho = \mathbf{F}_{\rho \mathbf{x}_g} \mathbf{x}_g + \nu_g \tag{3.13}$$

where ν_a and ν_g denote the accelerometer and gyro measurement noise, respectively. With these definitions, eqn. (3.8) can be expanded as

$$\begin{bmatrix} \delta\dot{\mathbf{p}} \\ \delta\dot{\mathbf{v}} \\ \delta\dot{\rho} \end{bmatrix} = \begin{bmatrix} \mathbf{F_{pp}} & \mathbf{F_{pv}} & \mathbf{F_{p\rho}} \\ \mathbf{F_{vp}} & \mathbf{F_{vv}} & \mathbf{F_{v\rho}} \\ \mathbf{F_{\rho p}} & \mathbf{F_{\rho v}} & \mathbf{F_{\rho\rho}} \end{bmatrix} \begin{bmatrix} \delta\mathbf{p} \\ \delta\mathbf{v} \\ \delta\rho \end{bmatrix} + \begin{bmatrix} \mathbf{0} & \mathbf{0} \\ \mathbf{F_{v x}}_a & \mathbf{0} \\ \mathbf{0} & \mathbf{F}_{\rho \mathbf{x}_g} \end{bmatrix} \begin{bmatrix} \mathbf{x}_a \\ \mathbf{x}_g \end{bmatrix} + \begin{bmatrix} \omega_{\mathbf{p}} \\ \omega_{\mathbf{v}} + \nu_a \\ \omega_\rho + \nu_g \end{bmatrix} \tag{3.14}$$

$$\begin{bmatrix} \delta\dot{\mathbf{p}} \\ \delta\dot{\mathbf{v}} \\ \delta\dot{\rho} \\ \dot{\mathbf{x}}_a \\ \dot{\mathbf{x}}_g \end{bmatrix} = \begin{bmatrix} \mathbf{F_{pp}} & \mathbf{F_{pv}} & \mathbf{F_{p\rho}} & \mathbf{0} & \mathbf{0} \\ \mathbf{F_{vp}} & \mathbf{F_{vv}} & \mathbf{F_{v\rho}} & \mathbf{F_{vx_a}} & \mathbf{0} \\ \mathbf{F_{\rho p}} & \mathbf{F_{\rho v}} & \mathbf{F_{\rho\rho}} & \mathbf{0} & \mathbf{F_{\rho x_g}} \\ \mathbf{0} & \mathbf{0} & \mathbf{0} & \mathbf{F_{x_a x_a}} & \mathbf{0} \\ \mathbf{0} & \mathbf{0} & \mathbf{0} & \mathbf{0} & \mathbf{F_{x_g x_g}} \end{bmatrix} \begin{bmatrix} \delta\mathbf{p} \\ \delta\mathbf{v} \\ \delta\rho \\ \mathbf{x}_a \\ \mathbf{x}_g \end{bmatrix} + \begin{bmatrix} \omega_{\mathbf{p}} \\ \omega_{\mathbf{v}} + \nu_a \\ \omega_\rho + \nu_g \\ \omega_{\mathbf{a}} \\ \omega_{\mathbf{g}} \end{bmatrix}. \tag{3.15}$$

In the implementation for this project, $\mathbf{x}_a$ and $\mathbf{x}_g$ represent accelerometer and gyro biases respectively. Modeling these biases as random walk processes, $\mathbf{F}_{\mathbf{x}_a\mathbf{x}_a}$ and $\mathbf{F}_{\mathbf{x}_g\mathbf{x}_g}$ are identically zero. By the chain rule,

$$\mathbf{F}_{\mathbf{v}\mathbf{x}_a} = \frac{\partial v}{\partial \mathbf{f}^p}\frac{\partial \mathbf{f}^p}{\partial \mathbf{x}_a} \tag{3.16}$$

$$= \mathbf{R}_{p2n}\frac{\partial \mathbf{f}^p}{\partial \mathbf{x}_a} \tag{3.17}$$

$$\mathbf{F}_{\rho\mathbf{x}_g} = \frac{\partial \rho}{\partial \omega_{ip}^p}\frac{\partial \omega_{ip}^p}{\partial \mathbf{x}_g} \tag{3.18}$$

$$= \mathbf{R}_{p2n}\frac{\partial \omega_{ip}^p}{\partial \mathbf{x}_g} \tag{3.19}$$

where the δ on the error quantities has been dropped throughout to simplify the notation. Finally, with the definitions stated above, $\frac{\partial \mathbf{f}^p}{\partial \mathbf{x}_a} = \frac{\partial \omega_{ip}^p}{\partial \mathbf{x}_g} = \mathbf{I}$.

The power spectral densities for the driving noise processes $\omega_{\mathbf{a}}$ and $\omega_{\mathbf{g}}$ were determined by analysis instrument biases over an extended period of time. Similarly, the spectral density of the measurement noise processes ν_a and ν_g were determined by the analysis of measurement data.

3.1.3 Numeric Integration

The INS equations are updated at 100 Hz, using a predictor–corrector integration routine. Given the equation

$$\dot{\mathbf{x}} = \mathbf{f}(\mathbf{x}, \mathbf{u}) \tag{3.20}$$

and the state $x(k)$ at the k-th iteration, the predictor corrector algorithm calculates the state at the (k+1)-st iteration in three steps:

Predictor Step: $x_p(k+1) = x(k) + f(x(k), u(k))dt$

Corrector Step: $x_c(k+1) = x(k) + f(x_p(k+1), u(k))dt$

Average: $x(k+1) = (x_p(k+1) + x_c(k+1))/2$

which is accurate to second order.

3.2 Differential Global Positioning (DGPS)

3.2.1 GPS Observables

The two basic outputs of a GPS receiver are pseudo-range and carrier phase data. A two frequency receiver will output range and phase measurements for each carrier frequency, resulting in four basic outputs.

Common Mode Errors	Standard Deviation
Selective Availability	24.0 m
Ionosphere	7.0 m
Clock and Ephemeris	3.6 m
Troposphere	0.7 m
Non-common Mode Errors	
Receiver Noise	0.1-0.7 m
Multipath	0.1-3.0 m

Table 3.1: Error due to Noise Sources

Combinations of these basic outputs provide other (sometimes) useful signals. The basic outputs and their combinations are discussed in the following subsections. These sections will serve as background for the description in Section 3.4 of the aided INS approach used in this project. The first subsection discusses the magnitude of various GPS measurement errors as a foundation for discussion in the subsequent sections.

GPS Error Sources

The discussion of the following sections will introduce various GPS measurement quantities and the errors that corrupt the measurements. This section provides a brief reference discussion of the various forms of error, to eliminate duplication in the following sections.

Table 3.1 (see Tables 3-1 and C-1 in [33]) lists typical standard deviations for the various sources of noise corrupting the GPS C/A code observables. Common mode error refers to those error sources that would be common to every receiver operating in a limited geographic region. Non-common mode errors refer to those errors that could be distinct to receivers operating even in close proximity. The actual amount of non-common mode noise will be dependent on receiver type and techniques used to mitigate against multipath effects. The magnitude of the non-common mode noise sources on the phase quantities would be significantly smaller than the values listed in Table 3.1 for the C/A code observables.

Based on the estimates of the standard deviation of the various noise sources contained in Table 3.1, standard GPS with selective availability active produces a range standard deviation error on the order of 25.27 m from common mode errors. Differential GPS is discussed in Section 3.2.2. Differential operation achieves significant accuracy improvements by canceling the effect of the common mode errors.

Selective availability is the deliberate corruption of the GPS system accuracy by agencies of the U.S. government. Selective availability can be implemented either by dithering of the satellite vehicle clocks or by corrupting the broadcast ephemeris data. Usually, the first form is used. Selective availability is scheduled to be removed between 2002 and 2006. Ionospheric error and tropospheric error are caused by the deviation of the speed of light when not traveling in a vacuum. The nature of the two errors are different, since the ionosphere is a dispersive medium. Clock and ephemeris errors represent the difference between the actual and computed satellite clock and position variables. All of these errors are slowly time varying and can be

effectively removed by the use of broadcast range corrections.

Pseudo-range Observables

Let the receiver clock offset from the satellite system time be denoted by Δt_r. The receiver clock offset is the error between the GPS system time and time measured on the receiver. The receiver clock offset exists due to drift in the local oscillator of the receiver.

With the three position variables and the clock error, there are four unknown quantities in the standard GPS positioning application. The GPS positioning problem is to determine these four unknowns based on the following system of equations, representing range measurements[1] from four different satellites:

$$\begin{aligned}
\tilde{\rho}^{(1)} &= ((X^{(1)}-x)^2+(Y^{(1)}-y)^2+(Z^{(1)}-z)^2)^{0.5} \\
&\quad +c\Delta t_r + c\Delta t_{sv}^{(1)} + c\Delta t_a^{(1)} + SA^{(1)} + E^{(1)} + MP^{(1)} + \eta^{(1)} \qquad (3.21)\\
\tilde{\rho}^{(2)} &= ((X^{(2)}-x)^2+(Y^{(2)}-y)^2+(Z^{(2)}-z)^2)^{0.5} \\
&\quad +c\Delta t_r + c\Delta t_{sv}^{(2)} + c\Delta t_a^{(2)} + SA^{(2)} + E^{(2)} + MP^{(2)} + \eta^{(2)} \qquad (3.22)\\
\tilde{\rho}^{(3)} &= ((X^{(3)}-x)^2+(Y^{(3)}-y)^2+(Z^{(3)}-z)^2)^{0.5} \\
&\quad +c\Delta t_r + c\Delta t_{sv}^{(3)} + c\Delta t_a^{(3)} + SA^{(3)} + E^{(3)} + MP^{(3)} + \eta^{(3)} \qquad (3.23)\\
\tilde{\rho}^{(4)} &= ((X^{(4)}-x)^2+(Y^{(4)}-y)^2+(Z^{(4)}-z)^2)^{0.5} \\
&\quad +c\Delta t_r + c\Delta t_{sv}^{(4)} + c\Delta t_a^{(4)} + SA^{(4)} + E^{(4)} + MP^{(4)} + \eta^{(4)} \qquad (3.24)
\end{aligned}$$

where $\tilde{\rho}^{(1)}$, $\tilde{\rho}^{(2)}$, $\tilde{\rho}^{(3)}$, and $\tilde{\rho}^{(4)}$ are the measured pseudo-ranges, $(X^{(i)}, Y^{(i)}, Z^{(i)})$ are the ECEF position coordinates of satellite i, (x, y, z) are the ECEF position coordinates of the receiver antenna, Δt_r is receiver clock bias, $\Delta t_{sv}^{(i)}$ is the clock bias of the satellite vehicle, $\Delta t_a^{(i)}$ is the atmospheric delay, $SA^{(i)}$ represents the deliberate corruption of the satellite signals under the policy of selective availability, $E^{(i)}$ represents error in the broadcast ephemeris data, $MP^{(i)}$ represents multipath error, $\eta^{(i)}$ represents receiver tracking error noise, and c is the speed of light. The $()^{(i)}$ notation refers to the quantity in parenthesis referenced to the i-th satellite.

Linearizing eqns. (3.21-3.24) gives

$$\begin{bmatrix} \tilde{\rho}^{(1)}(\mathbf{x}) \\ \tilde{\rho}^{(2)}(\mathbf{x}) \\ \tilde{\rho}^{(3)}(\mathbf{x}) \\ \tilde{\rho}^{(4)}(\mathbf{x}) \end{bmatrix} = \begin{bmatrix} \tilde{\rho}^{(1)}(\mathbf{x}_0) \\ \tilde{\rho}^{(2)}(\mathbf{x}_0) \\ \tilde{\rho}^{(3)}(\mathbf{x}_0) \\ \tilde{\rho}^{(4)}(\mathbf{x}_0) \end{bmatrix} + \mathbf{H} \begin{bmatrix} (x-x_0) \\ (y-y_0) \\ (z-z_0) \\ c\Delta t_r \end{bmatrix} + \begin{bmatrix} \chi^{(1)} \\ \chi^{(2)} \\ \chi^{(3)} \\ \chi^{(4)} \end{bmatrix} + h.o.t.'s \qquad (3.25)$$

where $\chi^{(i)}$ has been used as a shorthand to denote the terms $c\Delta t_{sv}^{(i)} + c\Delta t_a^{(i)} + SA^{(i)} + E^{(i)} + MP^{(i)} + \eta^{(i)}$ corrupting each measurement, (x_0, y_0, z_0) is the point of linearization, $h.o.t.'s$ represents the higher order terms in the expansion,

$$\rho^{(i)}(\mathbf{x}) = ((X^{(i)}-x)^2+(Y^{(i)}-y)^2+(Z^{(i)}-z)^2)^{0.5}, \qquad (3.26)$$

[1] Calculated as transit time multiplied by the speed of light.

and

$$\mathbf{H} = \left[\begin{array}{cccc} \frac{\delta\rho^{(1)}}{\delta x} & \frac{\delta\rho^{(1)}}{\delta y} & \frac{\delta\rho^{(1)}}{\delta z} & 1 \\ \frac{\delta\rho^{(2)}}{\delta x} & \frac{\delta\rho^{(2)}}{\delta y} & \frac{\delta\rho^{(2)}}{\delta z} & 1 \\ \frac{\delta\rho^{(3)}}{\delta x} & \frac{\delta\rho^{(3)}}{\delta y} & \frac{\delta\rho^{(3)}}{\delta z} & 1 \\ \frac{\delta\rho^{(4)}}{\delta x} & \frac{\delta\rho^{(4)}}{\delta y} & \frac{\delta\rho^{(4)}}{\delta z} & 1 \end{array} \right] \Bigg|_{(x_0,y_0,z_0)} \tag{3.27}$$

where

$$\begin{aligned} \frac{\delta\rho^{(i)}}{\delta x} &= \frac{-(X^{(i)}-x)}{((X^{(i)}-x)^2+(Y^{(i)}-y)^2+(Z^{(i)}-z)^2)^{0.5}} \\ \frac{\delta\rho^{(i)}}{\delta y} &= \frac{-(Y^{(i)}-y)}{((X^{(i)}-x)^2+(Y^{(i)}-y)^2+(Z^{(i)}-z)^2)^{0.5}} \\ \frac{\delta\rho^{(i)}}{\delta z} &= \frac{-(Z^{(i)}-z)}{((X^{(i)}-x)^2+(Y^{(i)}-y)^2+(Z^{(i)}-z)^2)^{0.5}}. \end{aligned}$$

For solution, each component eqn. of (3.25) can be written as[2]

$$\delta\hat{\rho}^{(i)} = \tilde{\rho}^{(i)}(x) - \hat{\rho}^{(i)}(\mathbf{x}_0) = \mathbf{h}^{(i)}\delta\mathbf{x} + \chi^{(i)} + h.o.t.'s \tag{3.28}$$

where the first three components of $\mathbf{h}^{(i)}$ (the i-th row of $\mathbf{H}$) form a unit vector pointing from $\mathbf{x}_0$ to the satellite.

In solving equations 3.21-3.24, the effective satellite vehicle (SV) positions are required. The position of the space vehicle antenna phase center in earth centered earth fixed (ECEF) coordinates can be computed using data derived from the GPS navigation messages as described in [1, 14].

Note that the position estimation accuracy will depend on both the numeric properties of $\mathbf{H}$ and the magnitude of χ.

Carrier Phase Observables

In addition to tracking the code, a receiver in phase lock on the carrier signal is able to track the relative phase shift in the carrier between any two time instants. Therefore, although the receiver cannot directly measure the number of carrier cycles between it and a given satellite, the receiver can measure the change in this number of cycles.

The carrier phase observable for the i-th satellite can be represented as

$$\begin{aligned} (\tilde{\phi}^{(i)} + N^{(i)})\lambda &= ((X^{(i)}-x)^2+(Y^{(i)}-y)^2+(Z^{(i)}-z)^2)^{0.5} \\ &\quad + c\Delta t_r + c\Delta t_{sv}^{(i)} - c\Delta t_a^{(i)} + SA^{(i)} + E^{(i)} + mp^{(i)} + \beta^{(i)} \qquad (3.29) \\ &= \rho^{(i)} + e_{cm}^{(i)} + mp^{(i)} + \beta^{(i)} \qquad (3.30) \end{aligned}$$

where $N^{(i)}$ is the integer phase ambiguity, λ is the carrier wavelength, $mp^{(i)}$ is the carrier signal multipath, $\beta^{(i)}$ is random measurement noise, and all other symbols are defined in eqn. (3.21). The interest in the carrier signal stems from the fact that the non-common mode errors $mp^{(i)}$ and $\beta^{(i)}$ are much smaller than the respective errors on the code observable ($\sigma_{mp} \approx 2cm.$ and $\sigma_\beta \approx 1mm.$). The common-mode errors are

[2] The measured pseudo-range should be corrected for satellite clock offset (Δt_{sv} [1])

essentially the same as those on the code observable, except that the ionospheric error enters eqns. (3.21) and (3.29) with opposite signs.

In the differential mode of operation (see Section 3.2.2), the common mode errors can be reduced to produce an observable accurate to a few centimeters. Let this differentially corrected phase be described as

$$\begin{aligned} \triangle\phi^{(i)}\lambda &= (\tilde{\phi}^{(i)} - \tilde{\phi}_o^{(i)})\lambda & (3.31) \\ &= \mathbf{h}^{(i)}(\mathbf{x} - \mathbf{x}_o) - \left(N^{(i)} - N_o^{(i)}\right)\lambda + (mp^{(i)} - mp_o^{(i)}) + (\beta^{(i)} - \beta_o^{(i)}) & (3.32) \end{aligned}$$

where the subscript in $(\zeta)_o^{(i)}$ refers the generic quantity ζ to the DGPS base station. The differentially corrected phase of eqn. (3.32) provides a very accurate measure of range, if the integer ambiguity can be determined.

The integer phase ambiguity is the whole number of carrier phase cycles between the receiver and satellite at an initial measurement time. It is a (usually large) unknown integer constant (barring cycle slips). To make use of carrier phase observable as a range estimate, the integer ambiguity must be estimated. Alternatively, the carrier phase measurement could be differenced across time epochs, eliminating the constant integer offset, to provide an accurate measurement of the change in range.

Doppler Carrier Phase Processing

Note that if eqn. (3.32) is differenced between two measurement times, an accurate measure of the change in satellite to receiver range results

$$(\triangle\phi^{(i)}(k) - \triangle\phi^{(i)}(k-1))\lambda = \mathbf{h}^{(i)}(k)\triangle x(k) - \mathbf{h}^{(i)}(k-1)\triangle x(k-1) + \delta mp_i(k) + \delta\beta_i(k) \quad (3.33)$$

where $\triangle x(k) = (x(k) - x_o(k))$, and the relative clock error is included in $\triangle x(k)$. If the relative acceleration of the base and rover is small during the differencing time, then a set of four 'Doppler' measurements can be processed to yield an accurate estimate of relative velocity

$$(\triangle\phi^{(i)}(k) - \triangle\phi^{(i)}(k-1))\lambda/dt = \mathbf{h}^{(i)}(k)\triangle v(k) + (\delta mp_i(k) + \delta\beta_i(k))/dt \quad (3.34)$$

where dt is the differencing time, and $\mathbf{h}^{(i)}(k) = \mathbf{h}^{(i)}(k-1)$ has been assumed. This assumption is accurate for small dt. If one antenna (the base) is known to be at rest, then earth relative velocity of the second antenna (the rover) results.

In the GPS literature, Doppler and carrier phase are also referred to as *delta range* and *integrated Doppler*, respectively. The latter are the more accurate names, as they describe the manner in which the measurements are actually made. Doppler is measured by the receiver as the change in phase (range) over a given time interval (i.e., delta range). Carrier phase is the integral of the delta ranges (i.e., integrated Doppler). Both measurements (Doppler and carrier phase) should not be used together, as they represent the same information. In choosing between the two there is a tradeoff. Carrier phase (once the integer ambiguity is resolved) gives a very accurate measure of range, but requires continuous phase lock. Loss of lock requires that the integers be re-estimated. Doppler gives a very accurate estimate of velocity only, but does not require continuous phase lock. Various methods have been suggested to utilize phase information (e.g., [5, 8, 18, 21, 22, 24, 27, 29]).

Wide and Narrow Lane Variables

This section develops the equations for the so called narrow-lane and wide-lane phase variables [23]. The interest in the wide-lane signal is that its wavelength is larger enough that the wide-lane variable is often used to facilitate the problem of integer ambiguity resolution.

The phase measurements of eqn. (3.32) at the L1 and L2 frequencies for a single satellite can be written as

$$(\tilde{\phi}_1 + N_1) = \frac{f_1}{c}r - \frac{f_2}{c}I_a + \frac{f_1}{c}(mp_1 + \beta_1) \tag{3.35}$$

$$(\tilde{\phi}_2 + N_2) = \frac{f_2}{c}r - \frac{f_1}{c}I_a + \frac{f_2}{c}(mp_2 + \beta_2) \tag{3.36}$$

where $\lambda_1 = \frac{c}{f_1}$ and $\lambda_2 = \frac{c}{f_2}$,the common mode errors have been eliminated through differential operation, and the $\triangle$'s have been dropped for convenience of notation. For small differential distances, the residual ionospheric error I_a should be small.

Forming the sum and difference of equations (3.35-3.36) results in

$$(\tilde{\phi}_1 + \tilde{\phi}_2) + (N_2 + N_1) = (\frac{f_1}{c} + \frac{f_2}{c})r - (\frac{f_2}{c} + \frac{f_1}{c})I_a + \frac{f_1}{c}(mp_1 + \beta_1) + \frac{f_2}{c}(mp_2 + \beta_2) \tag{3.37}$$

$$(\tilde{\phi}_1 - \tilde{\phi}_2) + (N_1 - N_2) = (\frac{f_1}{c} - \frac{f_2}{c})r - (\frac{f_2}{c} - \frac{f_1}{c})I_a + \frac{f_1}{c}(mp_1 + \beta_1) - \frac{f_2}{c}(mp_2 + \beta_2) \tag{3.38}$$

By defining

$$\lambda_w = \frac{c}{f1 - f2} \tag{3.39}$$

$$\lambda_n = \frac{c}{f1 + f2} \tag{3.40}$$

$$\tag{3.41}$$

eqns. (3.37) and (3.38) are written in meters as

$$(\tilde{\phi}_1 + \tilde{\phi}_2)\lambda_n = r - I_a - (N_2 + N_1)\lambda_n + \frac{\lambda_n}{\lambda_1}(mp_1 + \beta_1) + \frac{\lambda_n}{\lambda_2}(mp_2 + \beta_2) \tag{3.42}$$

$$(\tilde{\phi}_1 - \tilde{\phi}_2)\lambda_w = r + I_a - (N_1 - N_2)\lambda_w + \frac{\lambda_w}{\lambda_1}(mp_1 + \beta_1) - \frac{\lambda_w}{\lambda_2}(mp_2 + \beta_2) \tag{3.43}$$

The pseudo-range estimates can be processed similarly yielding

$$(\frac{\tilde{\rho}_1}{\lambda_1} - \frac{\rho_2}{\lambda_2})\lambda_w = r - I_a + \frac{\lambda_w}{\lambda_1}(MP_1 + \eta_1) - \frac{\lambda_w}{\lambda_2}(MP_2 + \eta_2) \tag{3.44}$$

$$(\frac{\tilde{\rho}_1}{\lambda_1} + \frac{\rho_2}{\lambda_2})\lambda_n = r + I_a + \frac{\lambda_n}{\lambda_1}(MP_1 + \eta_1) + \frac{\lambda_n}{\lambda_2}(MP_2 + \eta_2) \tag{3.45}$$

Note that the right hand sides of eqns. (3.43) and (3.45) are directly comparable. Since the residual ionospheric delay and the carrier noise are expected to be small and the coefficient of the code noise is significantly less than one, the difference of the two equations, described as

$$\begin{aligned}(\frac{\tilde{\rho}_1}{\lambda_1} + \frac{\tilde{\rho}_2}{\lambda_2})\lambda_n - (\tilde{\phi}_1 - \tilde{\phi}_2)\lambda_w = {} & (N_1 - N_2)\lambda_w + \frac{\lambda_n}{\lambda_1}(MP_1 + \eta_1) + \frac{\lambda_n}{\lambda_2}(MP_2 + \eta_2) \\ & - \frac{\lambda_w}{\lambda_1}(mp_1 + \beta_1) + \frac{\lambda_w}{\lambda_2}(mp_2 + \beta_2),\end{aligned} \tag{3.46}$$

should provide a basis for estimating the wide lane integer $(N_1 - N_2)$. The standard deviation of the noise on each estimate of $(N_1 - N_2)$ produced by eqn. (3.46) is approximately 0.7 times the code multipath in meters. Therefore, the correct integer ambiguity can be reasonably expected to be within three integers of the estimate from eqn. (3.46). Averaging of the above estimate of $(N_1 - N_2)$ does not significantly decrease the estimation error unless the sampling time is long (i.e., minutes) since the multipath is slowly time varying. Instead, an integer search will be required around the estimated value. Once this search is complete and $(N_1 - N_2)$ is determined, eqn. (3.43) is available for accurate carrier phase positioning and for aiding in direct estimation of the N_1 and N_2 variables.

Integer Ambiguity Resolution

Due to the dependence of eqn. (3.46) on the code measurement, which may be corrupted by significant levels of multipath, that equation is usually not used alone, but only to initialize an integer search. One such integer search approach based on least squares estimation and hypothesis testing [22, 39] is presented below. The method will be presented for a generic phase measurement and wavelength, and works equally well for any of the four phase variables previously discussed.

Consider a set of $n > 4$ differentially corrected phase measurements of wavelength λ

$$\begin{bmatrix} \tilde{\phi}_p \\ \tilde{\phi}_s \end{bmatrix} \lambda + \begin{bmatrix} \mathbf{N}_p \\ \mathbf{N}_s \end{bmatrix} \lambda = \begin{bmatrix} \mathbf{H}_p \\ \mathbf{H}_s \end{bmatrix} \mathbf{x} + \begin{bmatrix} \beta_p \\ \beta_s \end{bmatrix} \tag{3.47}$$

where the measurements are partitioned into a primary and a secondary measurement set. The ambiguity resolution algorithm proceeds by hypothesizing a set of integers for the primary set of measurements and using the secondary set of measurements as a test of each hypothesis. The primary set of measurements must have at least four satellites and these four should be selected to have a reasonable GDOP[3].

Assume also that at the initial algorithm step, $\mathbf{x} = 0$, $var(\beta) = R = \sigma_\beta I$, and $\sigma_x \gg \sigma_\beta$. These assumptions, although realistic are not necessary for the algorithm to work, but allow a theoretical basis for the algorithm derivation by the standard recursive least squares process.

The search algorithm will be implemented as a nested triple 'for' loop. Prior to initializing the loop, the following variables should be defined to minimize calculations within the loop:

$$\mathbf{x}_\phi = \mathbf{H}_p^{-1} \tilde{\phi}_p \tag{3.48}$$

$$B_p = \mathbf{H}_p^{-1} \lambda \tag{3.49}$$

$$K = \left(\mathbf{H}^T \mathbf{H}\right)^{-1} \mathbf{H}_s \tag{3.50}$$

The meaning of each variable is defined below.

The algorithm proceeds as follows:

1. Hypothesize a set of integers $\mathbf{N_p} = [0, N_2, N_3, N_4]^T$ for the primary measurements. Each of the three 'for' loops counts over a range of one of these three integers (i.e., $N_i, i = 2, 3, 4$). If m integer values on each side of a nominal integer are hypothesized, then the entire algorithm will iterated $(2m+1)^3$ times. The first integer is artificially set to zero to make the solution unique. Note that without this

[3] Geometric Dilution of Precision. Good GDOP implies that the measurement matrix $\mathbf{H}$ is well conditioned

assumption, all the integers and the clock bias estimate could be increased by one wavelength without affecting the position solution. The clock bias that results from the following algorithm is $c\Delta t_r - N_1\lambda$. If it is necessary that the code and phase clock estimates match, then N_1 can be estimated based on the average of the discrepancy.

2. For the hypothesized integer vector, calculate the resulting position

$$\begin{aligned} \mathbf{x_p} &= \mathbf{H}_p^{-1}(\tilde{\phi}_p + \mathbf{N_p})\lambda \\ &= \mathbf{x}_\phi + B_p\mathbf{N_p}. \end{aligned} \tag{3.51}$$

This position estimate has variance

$$\begin{aligned} \mathbf{P}_{xp}^{-1} &= \mathbf{H}_p^T \frac{1}{\sigma_\beta} I \mathbf{H}_p \\ \mathbf{P}_{xp} &= \sigma_\beta (\mathbf{H}_p^T \mathbf{H}_p)^{-1}. \end{aligned}$$

3. Predict a value for the secondary measurement using $\mathbf{x_p}$

$$\hat{\phi}_s = \frac{1}{\lambda}\mathbf{H}_s\mathbf{x_p}. \tag{3.52}$$

4. Calculate the residual between the predicted and measured secondary phase

$$\mathbf{r\hat{e}s}_{sp} = (\tilde{\phi}_s - \hat{\phi}_s). \tag{3.53}$$

This quantity is biased by the secondary integer, which is estimated as

$$\hat{\mathbf{N}}_s = -round(\mathbf{r\hat{e}s}_{sp}). \tag{3.54}$$

This choice of $\hat{\mathbf{N}}_s$ does not guarantee a minimal residual for the corrected position due to the possible ill-conditioning of $\mathbf{H}$, but is still used as the alternative is another search over $\hat{\mathbf{N}}_s$ to find the minimizing integer set.

5. Correct the secondary phase residual for the estimate secondary integer estimate and convert to meters

$$\mathbf{r\hat{e}s}_{sm} = (\mathbf{r\hat{e}s}_{sp} + \hat{\mathbf{N}}_s)\lambda. \tag{3.55}$$

6. Calculate the correction to $\mathbf{x_p}$ due to the secondary measurements. This requires calculation of the gain vector $\mathbf{K} = \mathbf{P}_{xs}\mathbf{H}_s^T\mathbf{R}^{-1}$. Using the standard recursive least squares equations,

$$\begin{aligned} \mathbf{P}_{xs}^{-1} &= \mathbf{P}_{xp}^{-1} + \mathbf{H}_s^T \frac{1}{\sigma_\beta} I \mathbf{H}_s \\ \mathbf{P}_{xs}^{-1} &= \mathbf{H}_p^T\mathbf{H}_p \frac{1}{\sigma_\beta} + \mathbf{H}_s^T\mathbf{H}_s \frac{1}{\sigma_\beta} \\ \mathbf{P}_{xs} &= \sigma_\beta (\mathbf{H}^T\mathbf{H})^{-1}. \end{aligned}$$

Therefore,

$$\mathbf{K} = \left(\mathbf{H}^T\mathbf{H}\right)^{-1}\mathbf{H}_s^T \tag{3.56}$$

and

$$\triangle\mathbf{x} = \mathbf{K}\mathbf{r\hat{e}s}_{sm} \tag{3.57}$$

7. Calculate the output residual of the position corrected by the secondary measurement

$$\triangle \mathbf{y} = \left(\begin{bmatrix} 0 \\ 0 \\ 0 \\ 0 \\ \mathbf{r\hat{e}s}_{sm} \end{bmatrix} - \mathbf{H} \triangle \mathbf{x} \right) \tag{3.58}$$

8. Calculate the χ-squared variable q associated with $\triangle \mathbf{y}$ and use it to evaluate the hypothesized integer N_p. The properly defined χ-squared variable q would account for the covariance matrix of $\triangle \mathbf{y}$ which is straightforward to calculate give $\mathbf{P}_{xs}$. However, due to the required number of on-line calculations the covariance matrix is dropped in favor of the following simpler calculation

$$q = \frac{\triangle \mathbf{y}^T \triangle \mathbf{y}}{n-4}. \tag{3.59}$$

If the hypothesized integer set N_p is correct, then q will be small. Depending on the number of satellites available, the noise level, and the satellite geometry it may take several iteration epochs to identify the correct integer set. In this process other criteria such as the previously estimated position, the position variance, and the size of N_s can also be used to eliminate candidate integer sets.

Note that the algorithm is equally valid for the L1, L2, and wide-lane frequencies. In the implementation of this project, the algorithm is used first to determine the wide-lane integers. Then, the increased position accuracy achieved using the wide-lane phase range facilitates the L1 or L2 integer initialization and search.

In the implementation of this project, the above algorithm is processed (in each mode: widelane, L1, or L2) until only a single vector integer candidate remains. The algorithm is then processed again using the identified integer vector as the initial condition until a single vector integer candidate remains. The integer vector is only accepted as correct if the output vector identically confirms (i.e., matches) the initial condition.

Once the correct integers are identified, a similar algorithm is run with q monitored to determine if cycle slips have occurred. Cycle slip detection is also implemented by comparing and monitoring the code, widelane phase, L1, and L2 ranges.

3.2.2 Differential GPS Operation

The common mode error sources described previously severely limit the accuracy attainable using GPS. These errors are generally not observable using a single receiver unless its position is already known. However, the common mode errors are the same for all receivers in a local area. Therefore, if the errors could be estimated by one receiver and broadcast to all other receivers, the GPS accuracy could be substantially improved. Three Differential GPS (DGPS) techniques are described in [14]. Range based differential GPS was selected for this implementation as this approach allows the most flexibility in a system involving multiple roving vehicles.

Differential GPS involves a GPS receiver/antenna at a location (x_o, y_o, z_o), a receiver/antenna at an unknown possibly changing position (x, y, z), a satellite at the calculated position (x_{sv}, y_{sv}, z_{sv}), and a communication medium from the first receiver to the second receiver. In the discussion of this section, the

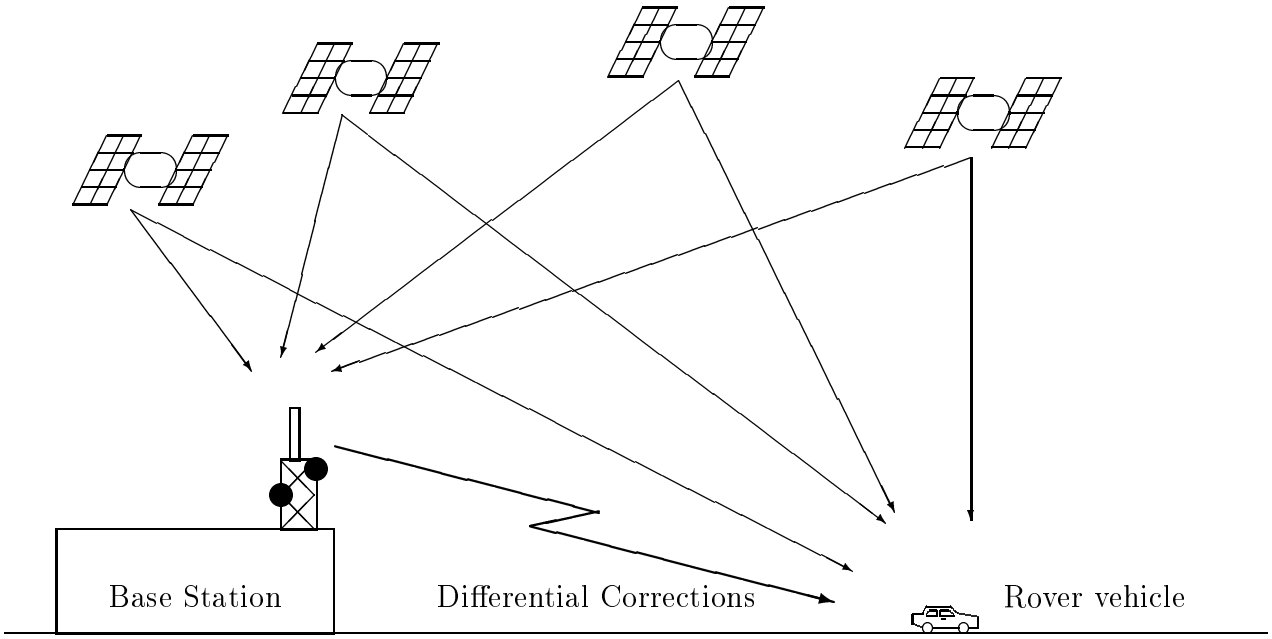

Figure 3.1: Differential GPS Scenario (Source: [20])

former receiver will be referred to as the *base*. The latter receiver will be referred to as the *rover*. A typical DGPS setup is illustrated in Figure 3.1. Note that one base station can service an unlimited number of roving vehicles. Also, wide area DGPS techniques are being developed which would allow a large area (e.g., the continental U.S.) to be served by a network of on the order of 10 base stations.

The correction equations of this subsection will be derived for a single satellite, but the process is identical for all satellites of interest. The derivation is also only presented for pseudo-range observables, but is also implementable for the L1, L2, and Doppler signals.

The GPS observables at the base and rover are, respectively, the pseudo-range measurements $\tilde{\rho}_o$ and $\tilde{\rho}_r$:

$$\tilde{\rho}_o = ((X-x_o)^2+(Y-y_o)^2+(Z-z_o)^2)^{0.5} + c\Delta t_o + c\Delta t_{sv} + c\Delta t_a + SA + E + MP_o + \eta_o \quad (3.60)$$

$$\tilde{\rho}_r = ((X-x_r)^2+(Y-y_r)^2+(Z-z_r)^2)^{0.5} + c\Delta t_r + c\Delta t_{sv} + c\Delta t_a + SA + E + MP_r + \eta_r \quad (3.61)$$

where the error terms are all defined as in eqn. (3.21) and the subscripts o and r denote the non-common mode errors corresponding to the base and rover respectively.

If the rover observable $\tilde{\rho}_r$ is replaced with $\tilde{\rho}_r - \tilde{\rho}_o$, the result is

$$\begin{aligned}\tilde{\rho}_r - \tilde{\rho}_o &= (r_r + c\Delta t^{sv} + SA + E + c\Delta t^a + MP_r + \eta_r) - (r_o + c\Delta t^{sv} + SA + E + c\Delta t^a + MP_o + \eta_o) \\ &= r_r - r_o + (MP_r + \eta_r) - (MP_o + \eta_o) \\ &= r_r - r_o + \eta \end{aligned} \quad (3.62)$$

where $r_r = \left((x_{sv}-x)^2+(y_{sv}-y)^2+(z_{sv}-z)^2\right)^{0.5} + c\Delta t_r$, $r_o = R_o + c\Delta t_{r_o}$,
$R_o = \left((x_{sv}-x_o)^2+(y_{sv}-y_o)^2+(z_{sv}-z_o)^2\right)^{0.5}$, and $\eta = (MP_r + \eta_r) - (MP_o + \eta_o)$. Note that r_o is calculatable due to the known location of the base receiver. The $c\Delta t_{r_o}$ term can be estimated and removed at the base station.

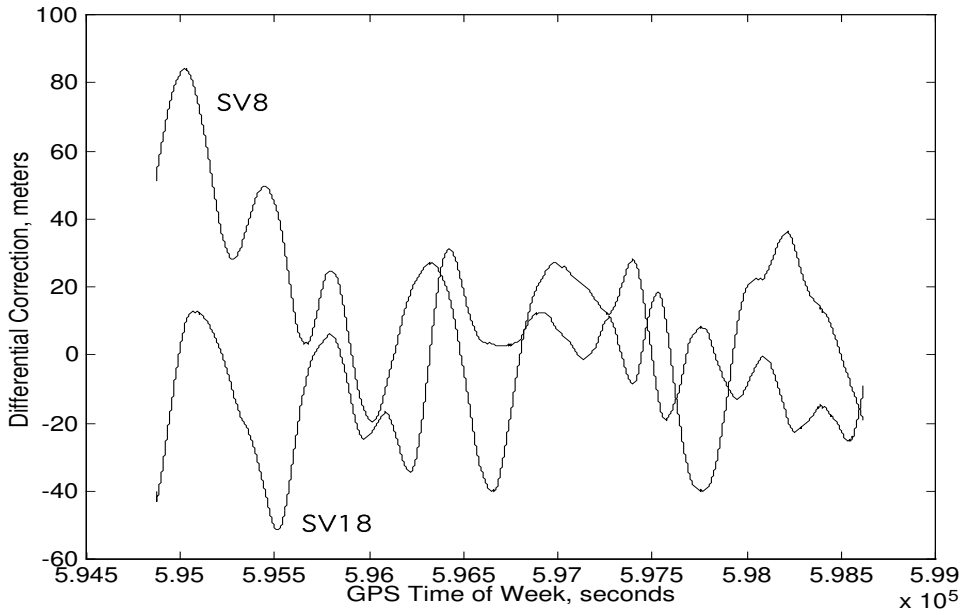

Figure 3.2: Example Differential Corrections

Since non-common mode noise η has a standard deviation between 0.1 and 4.0 m, depending on receiver design and multipath mitigation techniques, DGPS position accuracy is much better than standard GPS accuracy. Cancellation of the common mode noise sources in eqn. (3.62) assumes that the rover is sufficiently near (within 10-50 mi.) the base station and that the corrections are available at the rover in a timely fashion. Latency compensation is discussed in [34, 15]. Wide area DGPS techniques suitable for continent wide DGPS service are currently being developed [25].

The common mode noise sources are continuous and slowly time varying (see Figure 3.2) and have significant short term correlation (see Figure 3.3). Denote these common mode errors as $\Delta_{DGPS}(t)$ where

$$\Delta_{DGPS}(t) = -(c\Delta t_{sv}(t) + SA(t) + E(t) + c\Delta t_a(t)). \tag{3.63}$$

Note that $\Delta_{DGPS}(t)$ is straightforward to estimate at the base as $(r_o(t) - \rho_o(t)$. The correction Δ_{DGPS} is usually broadcast in range based differential GPS (DGPS) instead of ρ_o, as it is compensated for base receiver clock bias and its range is much smaller than that of ρ_o. Given that the corrections $\mathbf{\Delta}_{DGPS}$ are available at the rover for the satellites of interest, the DGPS positions are calculated as

$$\hat{\mathbf{x}} = (\hat{\mathbf{H}}^T\hat{\mathbf{H}})^{-1}\hat{\mathbf{H}}^T\left(\tilde{\rho} + \mathbf{\Delta_{DGPS}}\right). \tag{3.64}$$

To successfully implement a range space DGPS system, the base station must at a minimum broadcast the following set of information for each satellite: satellite id, range correction, ephemeris set identifier, and a reference time. A roving receiver then selects the most appropriate set of satellites for its circumstances. Normally, the base would also broadcast the range correction drift rate for each satellite to allow for latency compensation. For the implementation of this project, the base also broadcasts L1 and L2 phase corrections.

A main advantage of range space techniques is that the roving receiver can choose the best set of satellites for its circumstance. Implementation of a range space system however requires either that the user receiver

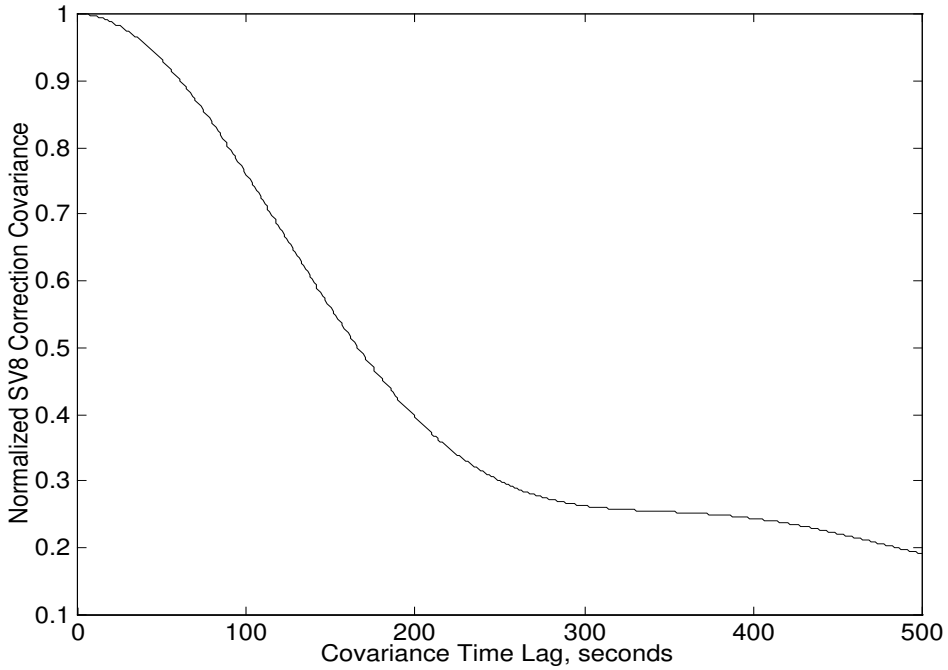

Figure 3.3: Normalized Covariance Sequence for the DGPS Corrections for SV8.

is "DGPS compatible" or that the user handle raw GPS data. DGPS compatible implies that the receiver is capable of being connected to a communication medium to receive and process DGPS range corrections.

3.3 DGPS Aided INS

Figure 3.4 shows a block diagram of the GPS aided INS implemented for this project. This implementation is referred to as a complementary filter. The noisy inertial measurement unit (IMU) outputs are processed by the INS. Since the INS is an integrative process, the output of the navigation system can be accurately modeled as the actual state plus a predominantly low frequency error. The INS output is processed to provide an estimate of the GPS measurement. The difference between the estimated GPS output and the measured GPS output is a signal that contains two noise components—the predominantly low frequency INS component and the predominantly high frequency GPS component. The frequency content of each noise component can be accurately modeled as described in the previous sections. The objective of the state estimation design is to attenuate the GPS measurement error and provide an accurate estimate of the INS state error denoted by δx. Therefore, the state estimator has a predominantly low pass characteristic. Subtracting the (Kalman filter) error estimate from the INS output, in a well designed system, produces an accurate estimate of the navigation state.

In the complementary filter approach, the INS is the primary navigation system which calculates the navigation state at the high rate at which it is used for control, guidance, and planning functions. The DGPS aiding information is used when it is available and satisfies conditions designed to verify proper sensor

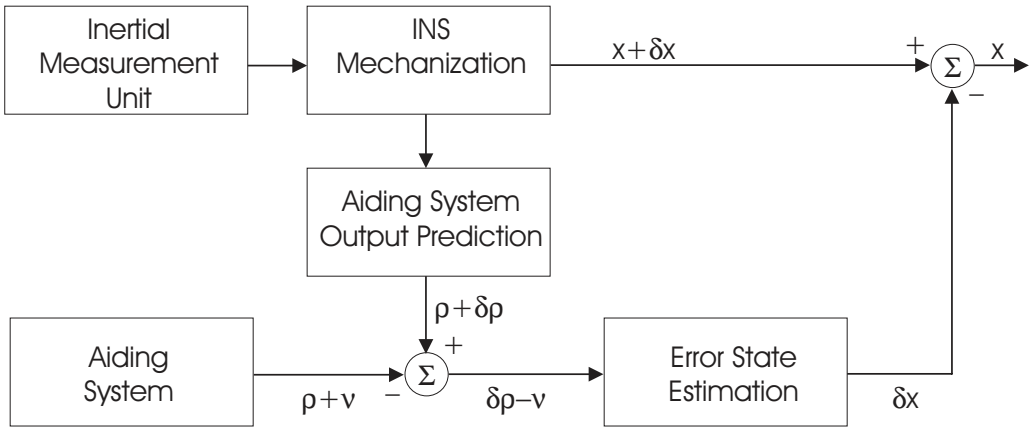

Figure 3.4: Complementary Filter

operation. When such aiding sensor information is not available or judged inaccurate, the INS continues its normal (unaided) operation (i.e., transformation and integration of the IMU outputs).

The error state estimator is implemented by a Kalman filter based on the linearized error dynamics presented in Section 3.1.2 and the linearized observation matrix of eqn. (3.27). All driving noise spectral density strengths were estimated from experimental data.

The two main advantages of the complementary filter approach selected for this implementation are that

1. the high rate INS navigation outputs are available regardless of the availability of the GPS aiding information;

2. the inputs to the Kalman filter can be accurately and properly modeled as stochastic processes, as appropriate for the technique; and,

3. the computationally intensive Kalman filter covariance propagation equations can be implemented at a low update rate even though the navigation state is calculated at the desired rate of the control system.

The complementary filter was implemented in 'feedback' configuration. This means that the INS state was corrected for the Kalman filter error estimates after each GPS update.

3.4 Overall System Design

Given the background of the previous sections, the overall design is fairly straightforward to describe.

3.4.1 Hardware Description

The inertial instruments consist of one three axis 2g accelerometer (manufactured by NeuwGhent Technology, Inc.), and three single-axis fiber optic gyros (Hitachi HGA-D). A photograph of the GPS antenna mounted

on the instrument platform is shown in Appendix B.

The 2g accelerometer range is too large for the lateral and longitudinal accelerations under typical conditions, but required for the vertical acceleration due to the nominal 1g gravitational acceleration. The accelerometer is an inexpensive solid state device which would be similar to the type of instrument expected in commercial automotive applications.

The gyros have a 10 Hz bandwidth and 60 degree per second input range. Both characteristics are reasonable for the expected application conditions. A larger bandwidth and input range may be required for emergency maneuvering. The input range must be carefully considered, as resolution and scale factor errors may become significant for large input ranges. The major drawback of the available set of gyros was the designer limited maximum sample rate of 50 Hz via a serial port connection. Although this is five times the sensor bandwidth, it still limits the (proper) INS update rate to 50 Hz. To achieve the desired implementation rate of 100 Hz with minimal delay, each sensed gyro output was assumed constant for two 0.01 s. sample periods.

Although these instruments were not ideally matched to the application, the project budget precluded purchasing alternative instruments. Even with the sensor deficiencies, the navigation system achieved the desired accuracies and the desired update rate was demonstrated. Overcoming the sensor deficiencies will only improve the demonstrated performance. Also, no special coding was required to achieve the results presented herein. Additional efforts in algorithm design could substantially increase the INS update and GPS correction rates.

For the experimental results shown later in the report, a compass and tilt meter manufactured by Precision Navigation were used to initialize the heading, roll, and pitch. The compass was not compensated for local magnetic fields. Even without these sensors, attitude error was rapidly (e.g., one trip around the parking lot) estimated by the Kalman filter. In a commercial application, logic to store and use the last best navigation estimates (prior to the ignition turning off) as the initial conditions for the next run could be considered. Given that the vehicle must be driven from its initial location (e.g., a parking lot) to the automated highway, the attitude errors should be observable and hence corrected by the navigation system; therefore, this sensor is not expected to be necessary in commercial applications.

Neither speedometer, odometer, nor brake pulse information was used in this implementation. Such information could be used and is available for free on many vehicles. Incorporating such signals would require extra computation for sensor calibration, but could provide both additional aiding and failure detection information.

The data acquisition system consists of an IBM 486 compatible with a National Instruments data acquisition board. GPS data was acquired from two Ashtech Z-12 Receivers via a serial port connection. The base station to rover serial port connection included a 19200 baud radio modem connection.

3.4.2 Software Description

The INS implemented a fixed tangent plane system at 100 Hz[4]. The origin was fixed at the location of the based station antenna phase center. The navigation states included: north, east, and vertical (up – positive) positions in meters; north, east, and down velocity in meters per second; roll, pitch, and yaw angles

[4] Higher rates could be achieved even with the current hardware and software.

in radians; receiver clock error and drift rate in meters and meters per second; platform frame gyro drift rates in radians per second; and, platform frame accelerometer bias in meters per second per second. The navigation error states were identical with the exception of the attitude errors. The estimate attitude errors were estimated in navigation frame as the north, east, and down tilt errors. The INS was implemented as an interrupt driven background process to ensure the designed update rate.

GPS aiding was implemented at a 1.0 Hz rate with scalar measurement processing. Four primary modes of GPS aiding were implemented:

1. INS only: This is the default mode of operation. Since INS is implemented as a background process, it will continue to run at 100 Hz regardless of the availability of aiding information. When GPS measurements are available, the software automatically switches to Mode 2.

2. Differential Pseudo-range: This is the default start-up mode. The primary objectives of this mode are to accurately estimate the navigation state errors and to switch to the widelane phase mode. Therefore, in this mode the system begins a search and verification process for the widelane integer ambiguities using the algorithm of Section 3.2.1 with $\lambda = \lambda_w$. In parallel with the integer ambiguity search, the Kalman filter estimates the navigation state on the basis of the differentially corrected pseudo-range measurements. In this mode, the measurement noise covariance for each measurement is set to $R = 2.0^2$ m^2. When the search process is complete, the software automatically switches to Mode 3.

3. Differential Widelane Phase: In this mode, the software attempts to estimate and verify the L1 integer ambiguities using the algorithm of Section 3.2.1 with $\lambda = \lambda_1$. In parallel with this integer search, the Kalman filter estimates the navigation state errors using the differentially corrected widelane phase measurements. In this mode, the measurement noise covariance for each measurement is set to $R = 0.1^2$ m^2. When this search process is complete, the software automatically switches to Mode 4. If widelock to at least four satellites is lost, the system automatically reverts to Mode 2.

4. Differential L1 Phase: This is the desired system operating mode. To be in this mode, the system will have estimated and verified the L1 integer ambiguities for at least four satellites. While in this mode, the Kalman filter will estimate the navigation error state using the differentially corrected L1 phase measurements. The measurement noise covariance for each L1 phase measurement is set to $R = 0.01^2$ m^2.

The INS is running in the background in all four modes. Also, the GPS measurement matrix in all GPS related modes is specified in equation (3.27). Analysis of the typical time to achieve each mode of operation is presented in Section 4.1.

In modes 3 and 4, the system monitors for loss of lock on each of the 'locked' satellites. If lock is lost on the satellite, then the Kalman filter will utilize the differentially corrected pseudo-range for that satellite instead of the corresponding phase measurement. The measurement information is correctly weighted by the Kalman filter by specification of the $\mathbf{R}$ matrix. As long as the system has lock to at least four satellites, it is usually able to correctly determine the integer ambiguities for 'unlocked' satellites by direct estimation instead of search. While in Mode 4, the system will search for L2 integer ambiguities. Once estimated, the L2 phase range is used as a consistency check on the L1 and widelane phase ranges. The consistency check is that the three ranges are statistically equal and that the integers satisfy $N_w = N_1 - N_2$.

In the Differential Pseudo-range Mode it is possible to also use the differentially corrected Doppler. This would allow on-the-fly (i.e., the vehicle could be moving) integer ambiguity resolution. The 9600 baud packet modem for this implementation could not accommodate Doppler corrections along with the pseudo-range, L1, and L2 corrections. Therefore, we assumed the vehicle was stopped in this mode, and synthesized a zero velocity 'measurement' with a corresponding value for the sensor uncertainty. This limitation (stationary vehicle) could be eliminated through a faster (or non-packet) modem, improved message formatting, or polynomial type correction prediction to decrease the required throughput..

The GPS receiver supplies a pulse aligned with the time of applicability of the GPS measurements. Receipt of this pulse by the INS computer causes the INS state to be saved and used for computation of the predicted GPS observables. The GPS measurements are received over the serial connection 0.4-0.6 seconds after the pulse (time of applicability). The delay is dependent on the number of satellites. Base corrections also transmitted serially do not arrive until approximately 0.7 seconds after the time of applicability of the GPS measurement. This left 0.3 seconds to complete the Kalman filter computation of the navigation error state and correct the navigation system prior to beginning the processing for the next measurement epoch.

Additional improvements which could be added include delay and lever arm compensation. In the approach described above, the navigation error state for each epoch is not available until approximately 0.8 seconds after its time of applicability. It is straightforward to propagate the error state from its time of applicability (i.e., t) to its time of availability (i.e., $t + 0.8$). This is most important at system initialization, since in steady state the errors are all quite small and slowly time varying. This delay compensation will be implemented in the near future.

The antenna phase center and accelerometer position do not coincide in most applications. For the platform for this project, the separation is approximately 0.6 meters. Therefore, the INS and GPS estimates of position and velocity will differ as the vehicle roll and pitch angles change. For example, a 10 degree roll or pitch error would result in 10 cm. of position error. Lever arm compensation can be achieved through a more involved algorithm for predicting the GPS outputs as a function of the INS state, and an alternative (fuller) measurement matrix. For higher accuracy, lever arm compensation can be implemented.

Chapter 4

Performance Analysis

Two methods were designed to test the positioning accuracy of the DGPS aided inertial navigation system. The primary variable of interest in the analysis, due to the focus on lateral control, was the lateral position accuracy. Accurate analysis of the positioning accuracy was difficult to achieve due to the lack of independent methods to measure ground truth at the centimeter level. Sections 4.2 and 4.3 describe system testing on a table top and on an amusement park ride, respectively. Section 4.1 analyzes the time from initialization to each mode of system operation.

4.1 Time to Phase Lock Analysis

This section describes an experiment that was designed to analyze the time required for the software to achieve each mode of phase lock described in Section 3.4.2. For each iteration of the experiment, the navigation system software was allowed to run normally until widelock, L1 lock, and L2 lock were all achieved and verified. At this point, the time that each lock status was achieved, the number of satellites, and the estimated position were written to a file. Then a software reset re-initialized the navigation system for the next iteration. The test was performed with a known baseline separation and the estimated position was use to verified correct integer lock.

In the 170 iterations used to generate the following data, there were no instances of incorrect phase lock. There was one 8 satellite iteration which did not achieve lock until approximately 900 seconds. This iteration was excluded from the statistical analysis.

Table 4.1 presents the statistics of the total time to achieve each mode of phase lock. Total time is measured from the instant at which the software reset occurs. This time includes a ten second period during which the system is in Mode 2 and using eqn. (3.46) to initialize the widelane integers. This estimate is used as the center of the initial integer search space. The indicated lock time is the time at which the integer ambiguities for that phase have been estimated and verified as previously described.

By these statistics, widelane accuracy would be available on average after 36 seconds. L1 accuracy would be available after 62 seconds. Note that the algorithm used allows the vehicle to be in motion during the search process if differential Doppler corrections are available. Therefore, as long as the average trip to the automated roadway requires in excess of 180 seconds, phase lock would be achieved. There is still the

	Widelock Time	L1 Lock Time	L2 Lock Time
Mean, 7 SV's	35.6	62.0	67.2
STD, 7 SV's	31.5	39.1	40.3
Mean, 8 SV's	40.5	60.1	65.9
STD, 8 SV's	33.9	38.5	38.6

Table 4.1: Statistics of the Time to Achieve each Mode of Phase Lock. Time is in Seconds from the Initial Turn on.

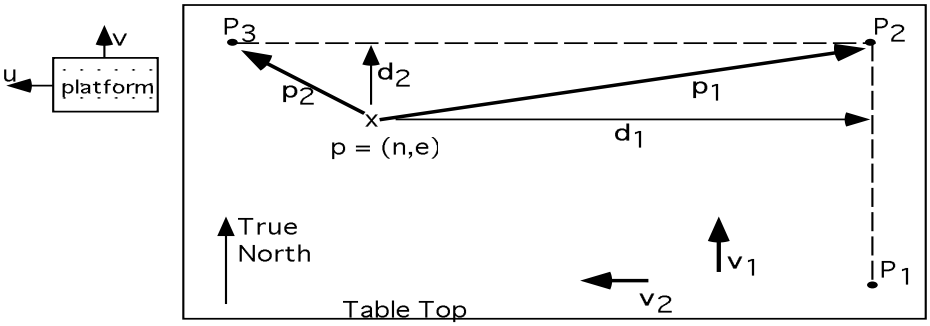

Figure 4.1: Experimental Set-up for Table Top Experiment.

potential for performance improvement in the area of integer search algorithms. The algorithm also works for six satellites, but does not work well for five satellites.

4.2 Table Top Testing

This section describes testing of the navigation system accuracy performed in a parking lot at UCR. The experiments involved two steps both completed while operating in Mode 4. First, the platform was attached to a car and driven around the parking lot for calibration purposes. Second, the platform was transferred to a table and translated repeatedly along two of the table sides. The second step provides a set of trajectories with lateral position accuracy repeatable to approximately one centimeter. Data for two independent repetitions of the experiment are included below.

After placing the navigation platform on the table top, it was cycled between three of the corners of the table, denoted P1, P2, and P3. Motion between the corners maintained a nominally constant heading and nominally kept one platform edge along a table edge. After moving between two points, the platform remained stationary at the destination point for approximately 10 s. During the table top portion of the experiment, INS data was recorded at 10 Hz. The table top set-up and various variables used in the subsequent analysis are illustrated in Figure 4.1. This figure also shows the nominal orientation of the platform and table relative to true north.

Following the experiment, all the stationary data (detected using a threshold of $\|v\| < 0.1\frac{m}{s}$) was sepa-

	N, m	E, m	D, m	$v_N, \frac{m}{s}$	$v_E, \frac{m}{s}$	$v_D, \frac{m}{s}$	ψ, rads.
P1 mean	59.8938	15.7627	5.5214	-0.0063	0.0058	-0.0112	-1.4649
P1 std.	0.0198	0.0203	0.0175	0.0157	0.0156	0.0115	0.0002
P2 mean	60.3189	15.7563	5.5259	-0.0110	-0.0053	-0.0124	-1.4642
P2 std.	0.0388	0.0241	0.0198	0.0315	0.0200	0.0129	0.0195
P3 mean	60.3468	14.4928	5.5520	-0.0074	0.0090	-0.0231	-1.4451
P3 std.	0.0275	0.0362	0.0173	0.0223	0.0301	0.0118	0.0095

Table 4.2: Mean and Standard Deviation of Estimated Corner Points for First Run

rated according to which of the three corner points was closest. The mean and standard deviation of the data for each corner is presented in Tables 4.2 and 4.3. Note the calculated standard deviations correspond well with the repeatability between the two data sets. Also, some of the deviation results from the experimenters having to maneuver the platform slowly near each corner to achieve the correct position and alignment.

Given the corner data for an experiment, two unit vectors were define so that $\mathbf{v}_1$ pointed from P1 to P2, and $\mathbf{v}_2$ pointed from P2 to P3. The off-track distance for the point $\mathbf{p} = (n, e)$ was calculated as follows:

$$\mathbf{p}_1 = P2 - \mathbf{p}, \text{ vector from } \mathbf{p} \text{ to P2} \tag{4.1}$$

$$\mathbf{p}_2 = P3 - \mathbf{p}, \text{ vector from } \mathbf{p} \text{ to P3} \tag{4.2}$$

$$\mathbf{d}_1 = \mathbf{p}_1 - (\mathbf{p}_1 \cdot \mathbf{v}_1)\mathbf{v}_1, \text{projection of } \mathbf{p}_1 \text{ perpendicular to } \mathbf{v}_1 \tag{4.3}$$

$$\mathbf{d}_2 = \mathbf{p}_2 - (\mathbf{p}_2 \cdot \mathbf{v}_2)\mathbf{v}_2, \text{projection of } \mathbf{p}_2 \text{ perpendicular to } \mathbf{v}_2 \tag{4.4}$$

$$e = sgn(p_{i1}v_{i2} - p_{i2}v_{i1})\|\mathbf{d}_i\| \text{ where i selects the vector } \mathbf{d}_1 \text{ or } \mathbf{d}_2 \text{ of smaller norm} \tag{4.5}$$

The sign of the third component of the cross product $\mathbf{p}_i \times \mathbf{v}_i$ has been used as a convenient means to keep track of the side of the path on which the estimated position is located.

Data relevant to the analysis of the off-track error is presented in Figures 4.2-4.7. Figures 4.2 and 4.5 present the off-track error versus time for the two experiments. The dashed line on these figures is the navigation system estimate of the off-track error standard deviation, immediately prior to the Kalman Filter correction, calculated at a one Hz rate. Figures 4.3 and 4.6 present a histogram of the off-track error. Figures

	N, m	E, m	D, m	$v_N, \frac{m}{s}$	$v_E, \frac{m}{s}$	$v_D, \frac{m}{s}$	ψ, rads.
P1 mean	59.8943	15.7606	5.5443	-0.0064	0.0025	0.0009	-1.5251
P1 std.	0.0379	0.0296	0.0242	0.0307	0.0214	0.0148	0.0449
P2 mean	60.3414	15.7503	5.5381	0.0050	-0.0143	-0.0106	-1.5088
P2 std.	0.0313	0.0241	0.0196	0.0246	0.0252	0.0130	0.0251
P3 mean	60.3478	14.4907	5.5616	-0.0056	0.0160	-0.0179	-1.5199
P3 std.	0.0243	0.0279	0.0228	0.0213	0.0276	0.0132	0.0260

Table 4.3: Mean and Standard Deviation of Estimated Corner Points for Second Run

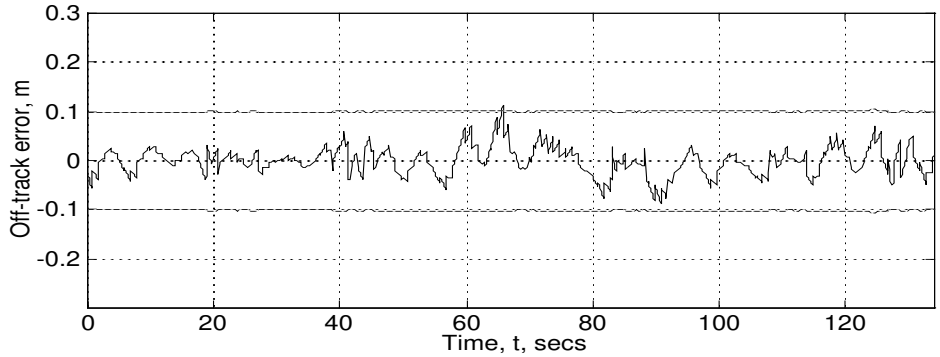

Figure 4.2: Table Top Navigation Test 1. Off-track Error versus Time.

4.4 and 4.7 present the platform speed versus time.

The first experiment involved motion from P1 to P2 and four round trip maneuvers between P2 and P3. The second experiment involved motion from P1 to P2, five round trip maneuvers between P2 and P3, and motion from P2 to P1. The long side of the table is represented by the line between P1 and P2.

For the first run of the experiment, the overall standard deviation of the off-track error was 0.0280 m. For the second run the off-track error standard deviation was 0.0364 m. This off-track error includes the effects of erroneous motion by the experimenters and multipath. No special multi-path precautions were used.

4.3 Amusement Park Ride Testing

This section describes testing of the navigation system accuracy performed at a local amusement park (Castle Park) on the 'Wipeout' ride. For this experiment, the instrument platform was attached (using bungee cords) to the back of the car. Batteries, computer equipment, and modems were loaded on the car floor, see the photos in Appendix B. The ride has three intended types of rotational motion, as shown in Figure 4.8. In normal operation, θ is extended to greater than 45 degrees while the ride spins around the ω_1 and ω_2 axes. For the experiments described below, θ and ω_2 are nominally both zero. The ride still does not sit level, as the ω_2 axis is not normal to the earth surface. The relative incline of the ride is about fifteen degrees. With θ fixed and ω_2 nominally zero, the ride trajectory will nominally be a circle in three space for non-zero ω_1. Photographs of the ride and its immediate surroundings are included in Appendix B.

The ride operator is only able to cycle the ride on or off. When on, the ride accelerates ω_1 to a rate that would saturate the gyros. When the key is off, the ride automatically applies breaking to slow the ride. Therefore, for these experiments, the operator had to alternately cycle the ride off and on to keep the ride spinning, but at a reasonable rate. This cycling of the ride is expected to cause mechanical movement and vibration which will cause the actual trajectory to deviate from the nominal circle.

In the results that follow, no special precautions were taken either at the base or rover to accommodate multipath effects. Multipath effects should be significant due to the large number of metal surfaces within the amusement park.

The navigation system accuracy is analyzed by comparing the navigation system position estimates to

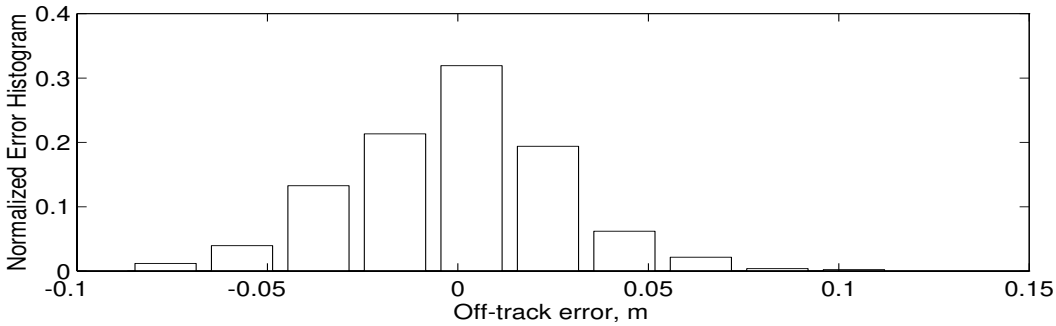

Figure 4.3: Table Top Navigation Test 1. Histogram of Off-track Error

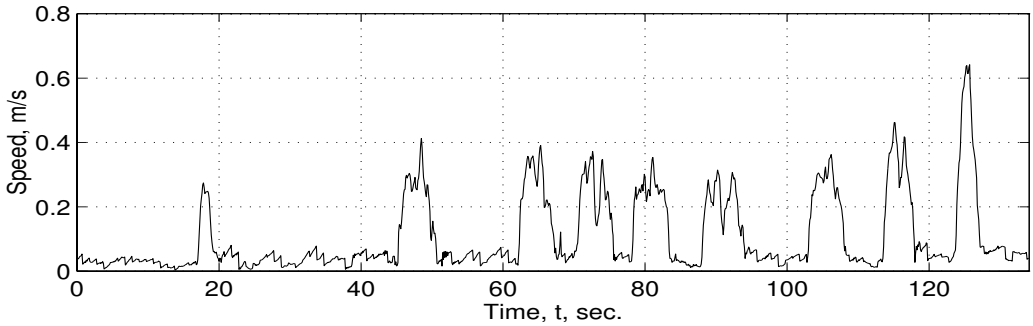

Figure 4.4: Table Top Navigation Test 1. Speed versus Time

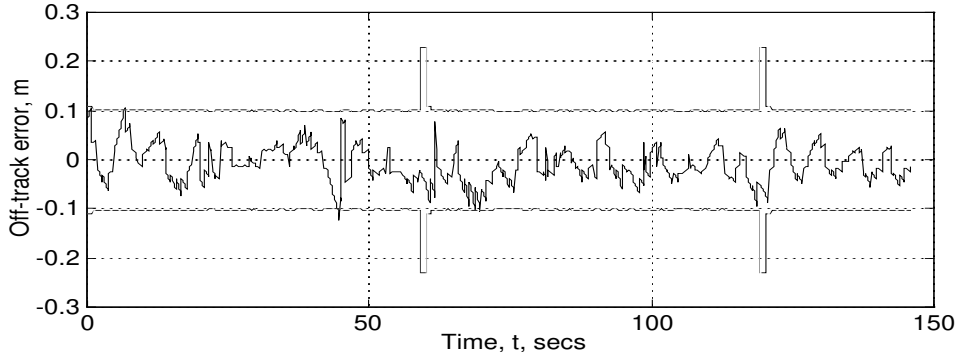

Figure 4.5: Table Top Navigation Test 2. Off-track Error versus Time.

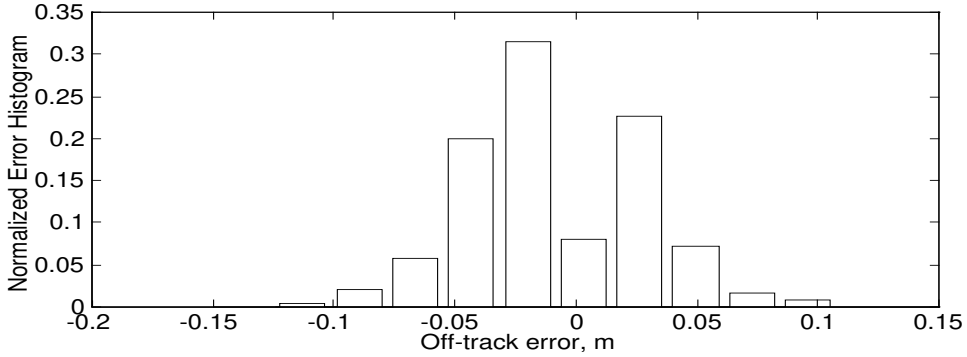

Figure 4.6: Table Top Navigation Test 2. Histogram of Off-track Error

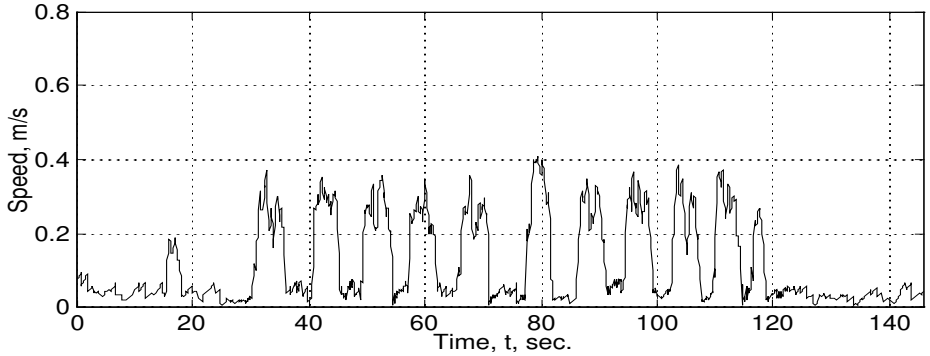

Figure 4.7: Table Top Navigation Test 2. Speed versus Time

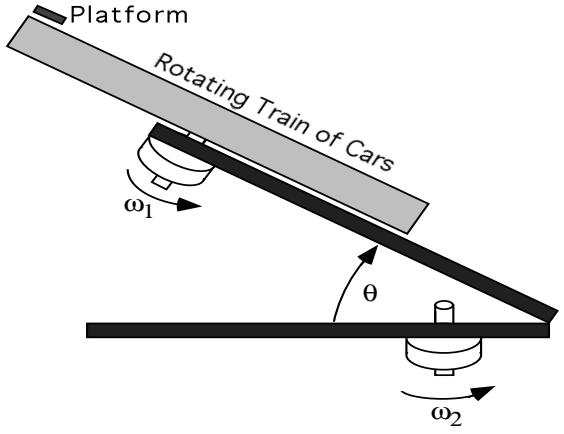

Figure 4.8: Wipeout Ride Mechanical Configuration.

Run	n_0, m.	e_0, m.	a, m.	b, m.	c, $\frac{1}{m^2}$
Widelane	-3.43	-8.11	3.56	3.54	0.0011
L1, Test 1	-6.79	-7.65	3.61	3.61	0.0000
L1, Test 2	-6.71	-7.64	3.57	3.60	0.0010

Table 4.4: Ellipse Trajectory Fit Parameters

a curve fit representing the nominal trajectory. The ride trajectory is nominally a circle in a plane inclined relative to a level plane. The projection of this circle onto the level plane will be an ellipse. Therefore, the analysis proceeds by first determining a best fit ellipse to the trajectory data and then analyzing the discrepancy of the navigation trajectory estimates from the best fit ellipse.

The form of the ellipse equation used in the analysis is

$$\frac{b}{a}(n-n_0)^2 + \frac{a}{b}(e-e_0)^2 + a \cdot b \cdot c(n-n_0)(e-e_0) = a \cdot b \tag{4.6}$$

which involves the five unknowns (a, b, c, n_0, e_0). The center parameters (n_0, e_0) were determined as the first two components of the center of a sphere that best fit the data. Then, with (n_0, e_0) fixed, a linear estimation problem can be defined to estimate the parameters (a, b, c) for the nominal tangent plane elliptic fit to the trajectory data.

Three data sets were acquired. Two of the data sets used L1 carrier phase aiding. One of the data sets used widelane carrier phase aiding. Figures corresponding to one of the L1 data sets and the widelane data set are included. The results of the trajectory curve fitting are displayed in Table 4.4. Note that the ride was rotated around the ω_2 axis between the L1 and widelane experiments, so the estimated center positions of the two sets of experiments do not match.

Off trajectory error was evaluated as

$$\epsilon = \frac{b}{a}(n-n_0)^2 + \frac{a}{b}(e-e_0)^2 + a \cdot b \cdot c(n-n_0)(e-e_0) - a \cdot b. \tag{4.7}$$

Since the lengths of the major and minor ellipse axes are essentially the same, this error can be considered the deviation of the navigation system position from a circle of known radius (i.e., off track error).

The major source of error in this experiment is mechanical motion, vibration, and flex of the ride which causes the actual path to deviate from its assumed elliptic shape. In addition to the three degrees of rotational freedom shown in Figure 4.8, the lever arm, rotational axes, and car are not perfectly rigid and fixed as the unbalanced disk rotates. Also, the torques necessary to accelerate and deaccelerate the ride as the operator cycles it off and on may cause distortion of the ideal trajectory. Therefore, a significant (but unquantifiable) portion of the error ϵ is caused by the actual trajectory deviating from the assumed ellipse, not by navigation system error.

Figure 4.9 displays the off trajectory error versus time for the first L1 experiment. The figure also shows the navigation system estimate of the off-track error standard deviation at a one Hz rate, calculated immediately prior to the Kalman filter measurement update. Figure 4.10 displays a normalized histogram of the off trajectory error. The standard deviation of ϵ for this L1 experiment was 5.98 cm. This total

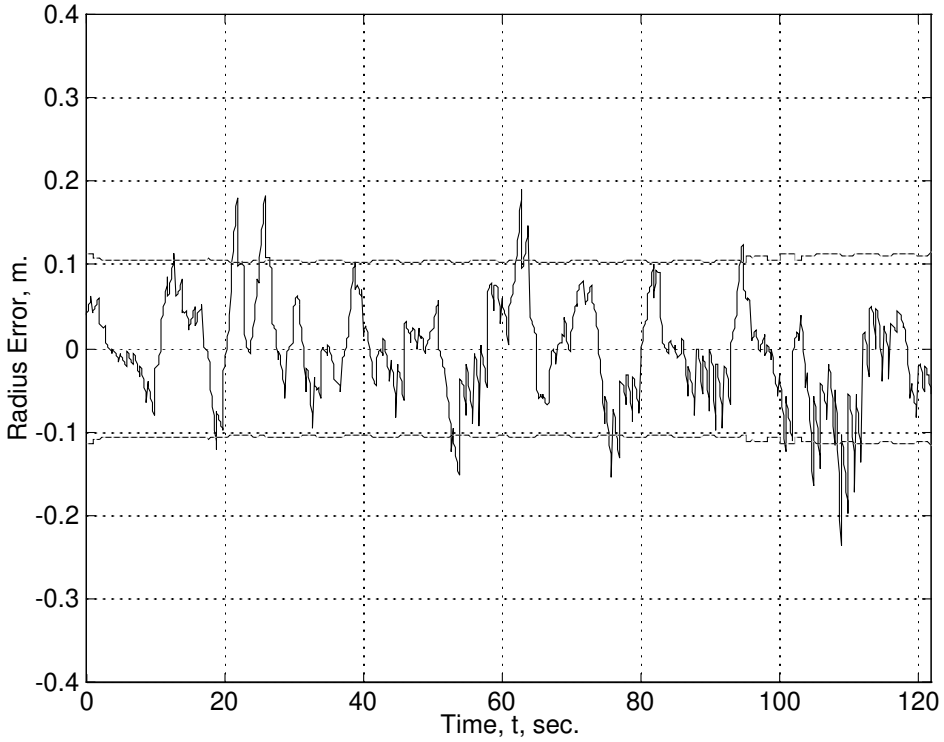

Figure 4.9: Amusement Park Ride L1 Test. Radius Error versus Time.

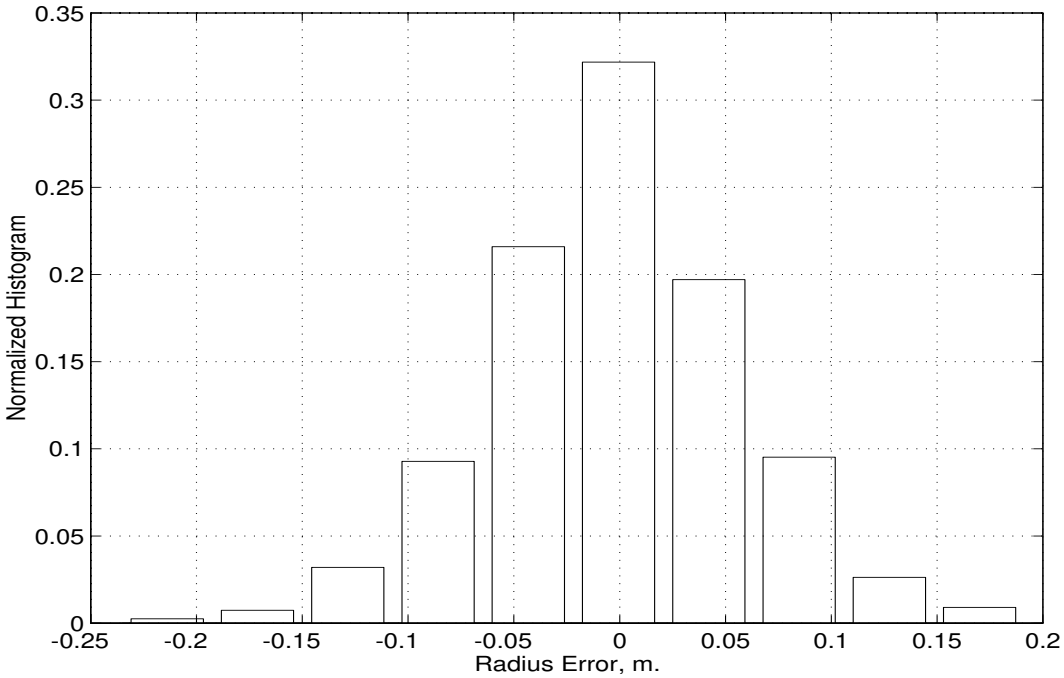

Figure 4.10: Amusement Park Ride L1 Test. Radius Error Histogram.

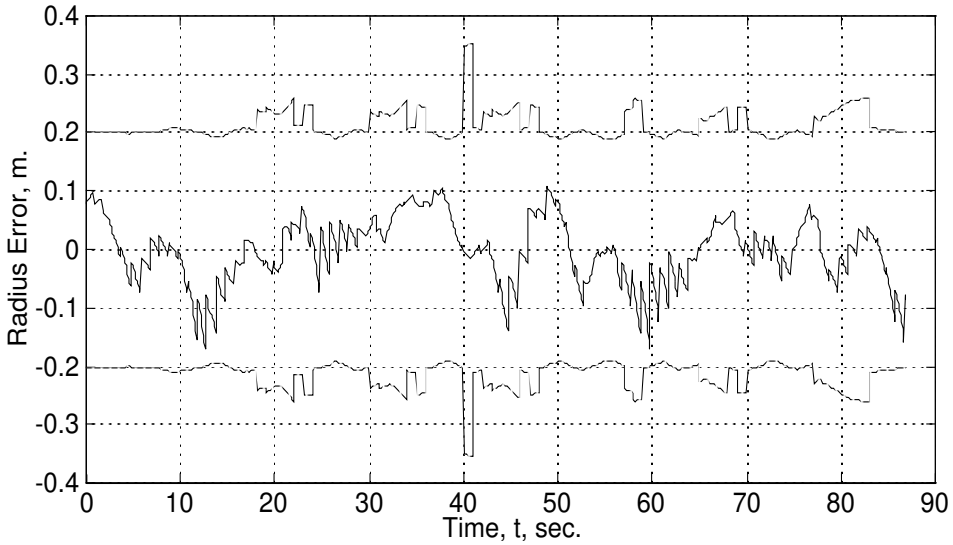

Figure 4.11: Amusement Park Ride Widelane Test. Radius Error versus Time.

standard deviation would be explained by 5 cm of ride standard deviation root sum squared with the 2.5 cm of L1 phase GPS standard deviation observed in the table top experiments. Five centimeters of mechanical motion deviation from the least squares trajectory is very reasonable

Figure 4.11 displays the off trajectory error versus time for the widelane experiment. The figure also shows the navigation system estimate of the off-track error standard deviation at a one Hz rate, calculated immediately prior to the Kalman filter measurement update. Figure 4.12 displays a normalized histogram of the off trajectory error. The standard deviation of ϵ for this widelane experiment was 5.50 cm. The widelane GPS position error standard deviation is expected to be ≈ 5.6 times that of the L1 phase GPS error standard deviation by eqn. (3.43). The fact that the errors in the two experiments are nearly identical in magnitude indicates that there is a more dominant error source such as the mechanical motion of the ride not exactly following an elliptic path.

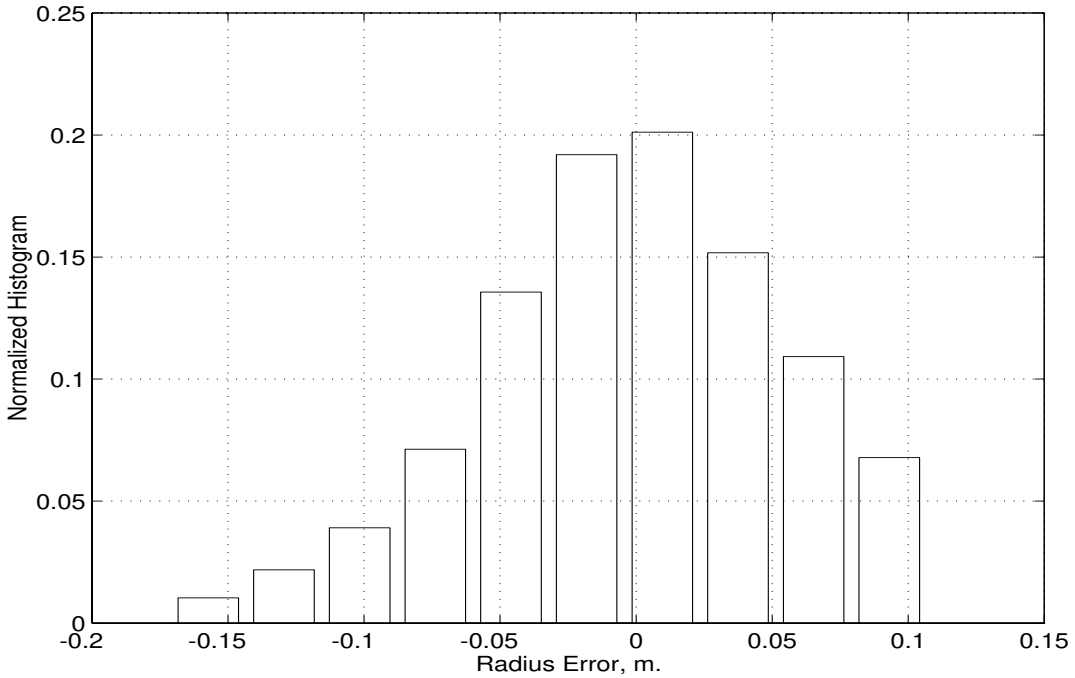

Figure 4.12: Amusement Park Ride Widelane Test. Radius Error Histogram.

Chapter 5

Conclusions and Future Research

This project has achieved its objective of implementing a DGPS aided INS system with a 100 Hz update rate and centimeter level accuracy. The exact position accuracy achieved is difficult to quantify due to the difficulty of obtaining a second ground truth measurement accurate to at least the centimeter level. The table top evaluation described herein demonstrates an accuracy of approximately 2.5 centimeter, with no special precautions taken to mitigate multipath effects. The amusement park ride demonstration demonstrated that the position accuracy was better than 6.0 cm, but beyond this level the navigation system error could not be discriminated from the mechanical system trajectory error.

As described in the following section, better accuracy can be achieved by research in several directions. Higher update rates are definitely achievable.

5.1 Future Research

Several directions are available for future research:

1. Integration of this stand alone navigation system into the PATH vehicles. This would have several benefits. First, PATH researchers would be able to use the results of this PATH funded research. The results of this project and existing magnetic and vision based positioning systems could be used synergistically. This would allow more accurate analysis of positioning accuracy, development and evaluation of vehicle control performance with additional navigation state information, and enhanced fault accommodation. Second, GPS aided INS navigation provides the full vehicle state and control preview information at update rates high enough to enable advanced control methods.

2. INS performance could be enhanced in several ways.

   (a) Delay compensation should be added to account for the latency between the time of applicability of the Kalman filter error estimates and their time of availability. The delay compensation is not critical, since the error states are slowly changing, but the fix is easy and will improve performance.

   (b) Lever arm compensation should be added to account for the ≈ 0.5 meter antenna phase center to accelerometer lever arm. The lever arm compensation is slightly more involved than the delay

compensation, but straightforward. This improvement should increase the observability of the attitude error and increase the position estimation accuracy when the vehicle is rolled or pitched.

(c) The INS update could still increase above 100 Hz. We did not implement special algorithms for higher updates, as our gyros could only be sampled at 50 Hz. The gyros should be replaced with gyros more typical of those which would be used in the final commercial application. In the process, the INS could be switched to a higher update rate and a quaternion implementation. The quaternions implementation is written, but was not integrated into the INS due to time and funding constraints.

3. The GPS performance could be improved by the following.

(a) The GPS update rate could also be increased. Although our receivers have a maximum 2 Hz update rate and a 0.3 second latency, receivers are now available with 20 Hz update rates and milliseconds of latency. In addition to the receiver latency, our differential corrections were delayed by 0.7 seconds due to computation and communication bandwidth constraints. It was this differential correction delay that limited the GPS update rate to 1 Hz. A higher bandwidth communication channel or improved base station design would have allowed correction information to be broadcast at higher rates and with shorter latency. Correction rate information would have allowed the communication channel delay to be compensated. The base station design is described in Chapter 7 of [14], but its implementation was not within the scope of this project.

(b) The correction rate information would also have allowed the use of differential Doppler observables. This would allow integer phase ambiguities to be estimated while the vehicle was in motion. This would be a very useful area for future research.

(c) Advanced integer ambiguity resolution techniques would decrease the time required to determine and verify the correct integers.

(d) Dynamic system fault detection techniques could be applied to reliably monitor for the loss of phase lock.

The IMU platform for this project was crude by typical INS standards. In this preliminary effort, the PI's did not use special test labs or manufacturing facilities for accurate system calibration and alignment. Still, very accurate navigation accuracy was achieved. Better accuracy should be achievable at low cost with a well designed automated manufacturing process which (1) places each instrument on the platform in a repeatable fashion; (2) performs an automated set of simple calibration procedures of each platform; and, (3) stores the calibration parameters in on board ROM. Such a process is not unreasonable for the high volume production that could be expected in the automotive industry.

5.2 Publications Resulting from this Project

At least two publications, which were partially funded by this project, are expected.

The first publication is reference [14]. This book is under contract, in the production stage, for publication with McGraw-Hill. The book provides an indepth discussion of the theory and design of GPS aided inertial navigation systems. The final draft of this text was submitted to McGraw-Hill in April 1998.

The second publication is a journal article, still in preparation, which describes the design and analysis results of this project. It will be submitted to either *IEEE Transactions on Vehicular Technologies*, *IEEE Tansactions on Control Systems Technology*, or the *Journal of Navigation*. This article is in its final draft stage.

Bibliography

[1] "Navstar GPS Interface Control Document," Report #ICD-GPS-200B-PR, Joint GPS Program Office, 1991.

[2] Anderson, J. and S. Lazar, "Lm and Lc: How the Military and Civilian Users of GPS can Share our Existing Spectrum," ION GPS 97 Presentation, September 18, 1997, Kansas City, MO. See also 'http://www.laafb.af.mil/SMC/CZ/homepage/lm/overview.htm'

[3] Bancroft, S., "An Algebraic Solution of the GPS Equations," *IEEE Transactions Aerospace and Electronic Systems,* Vol. AES-21, No. 7, Jan 1985, pp. 56-59.

[4] M. Barth and E. Johnston, "Using GPS Technology to Obtain Accurate Speed, Acceleration, and Grade Information for On-Road Emissions Measurement", in Fifth CRC On-Road Vehicle Emissions Workshop, San Diego, CA, 1995.

[5] Blomenhofer, H., G. Hein, E. Blomenhofer, and W. Werner, "Development of a Real-Time DGPS System in the Centimeter Range," *IEEE 1994 Position, Location, and Navigation Symposium*, Las Vegas, NV, 1994, pp. 532-539.

[6] Britting, K. R., *Inertial Navigation Systems Analysis*, Wiley-Interscience, New York, 1971.

[7] Brown, R. G., Y.C. Hwang, *Introduction to Random Signals and Applied Kalman Filtering*, 2nd ed. New York : J. Wiley, c1992.

[8] Cannon, E. "High-Accuracy GPS Semikinematic Positioning: Modeling and Results," *Navigation: Journal of the Institute of Navigation*, Vol. 37, No. 1, Summer 1990, pp. 53-64.

[9] W. Cormier and R. Fenton, "On the Steering of Automated VehiclesA Velocity Adaptive Controller," *IEEE Trans. on Vehicular Technology*, Vol. 29, no.4, pp. 375-385, 1980.

[10] R. T. Dunlay, "Obstacle avoidance perception processing for the autonomous land vehicle," in Proceedings of the IEEE International Conference on Robotics and Automation, pp. 912-917, 1987.

[11] E. Dickmanns and B. Mysliwetz, "Recursive 3-D road and relative ego-state recognition," *IEEE Transactions on Pattern Analysis and Machine Intelligence*, Vol. 14, pp. 199-213, 1992.

[12] [23] H. Euler, "Achieving High-Accuracy Relative Position in Real-time: System Design, Performance, and Real-Time Results," in IEEE 1994 Position Location and Navigation Symposium, Las Vegas, NV, USA, pp. 540-546, 1994.

[13] Fang, B. T., "Trilateration and Extension fo Global Positioning System Navigation," *Journal of Guidance, COntrol, and Dynamics*, Vol. 9, No. 6, Nov./Dec. 1986, pp. 715-717.

[14] Farrell, J. and M. Barth, *The Global Positioning System and Inertial Navigation: Theory and Practice*, In Preperation, expected publication in 1998.

[15] Farrell, J., M. Djodat, M. Barth, and M. Grewal, "Latency Compensation for Differential GPS," *Navigation: Journal of the Institute of Navigation*, Vol. 44, No. 1, Spring 1997, 99-107.

[16] R. Fenton and R. Mayhan, "Automated Highway Studies at The Ohio State UniversityAn Overview," *IEEE Trans. on Vehicular Technology*, Vol. 40, no.1, pp. 100-113, 1991.

[17] R. Fenton, G. Melocik, and K. Olson, "On the Steering of Automated Vehicles: Theory and Experiment," *IEEE Transactions of Automatic Control*, Vol. 21, no.3, pp. 306-315, 1976.

[18] Frodge, S.,S. Deloach, B. Remondi, D. Lapucha, and R. Barker, "Real-Time on-the-Fly Kinematic GPS System Results," *Navigation: Journal of the Institute of Navigation*, Vol. 41, No. 2, Summer 1994, pp. 175-186.

[19] A. Hanson, E. Riseman, and C. Weems, "Progress in computer vision at the University of Massachusetts," in DARPA Image Understanding Workshop, pp. 39-47, 1993.

[20] Grissom, L. "DGPS Correction Communication System Design," EE Senior Design Report, University of California, Riverside, June 1995.

[21] Hatch, R., "The Synergism of GPS Code and Carrier Measurements," Proc. 3rd Int. Geodetic Symposium on Sat. Doppler Pos., 1982, Las Cruces, NM.

[22] Hatch, R., "Instantaneous Ambiguity Resolution," Symposium No. 107, Kinematic Systems in Geodesy, Surveying and Remote Sensing, Banff, Canada, September 10-13, 1990, pp. 299-308, Springer Verlag.

[23] Hatch, R., "The Promise of a Third Frequency," *GPS World*, May 1996, pp. 55-58.

[24] Hwang, P. and R. Brown, "GPS Navigation: Combining Pseudorange with Continuous Carrier Phase using a Kalman Filter," *Navigation: Journal of the Institute of Navigation*, Vol. 37, No. 2, Summer 1990, pp. 181-196.

[25] C. Kee and B. Parkinson, "Wide Area Differential GPS as a Future Navigation System in the US," in IEEE 1994 Position Location and Navigation Symposium, Las Vegas, NV, USA, pp. 788-795, 1994.

[26] Kuan, Phipps, and Hsueh, "Autonomous Robotic Vehicle Road Following," *IEEE Transactions on Pattern Analysis and Machine Intelligence*, Vol. 10, pp. 648-658, 1988.

[27] Lachapelle, G., M. Cannon, and G. Lu, "High-Precision GPS Navigation with Emphasis on Carrier-Phase Ambiguity Resolution," *Marine Geodesy*, 15, pp. 253-269, 1992.

[28] Leva, J., "An Alternative Closed Form Solution to the GPS Pseudorange Equations," *Institute of Navigation (ION) National Technical Meeting*, Anahiem, CA, Jan. 1995.

[29] Mader, G., "Dynamic Positioning using GPS Carrier Phase Measurements," *Manuscripta Geodetica*, Springer-Verlag, Vol. 11, 1986, pp. 272-277.

[30] I. Masaki, Vision-Based Vehicle Guidance, New York: Springer-Verlag, 1992.

[31] R. Mayhan and R. Bishel, "A Two-Frequency Radar for Vehicle Automatic Lateral Control," *IEEE Trans. on Vehicular Technology*, Vol. 31, no.1, pp. 32-39, 1982.

[32] J. Meyer-Hilberg and T. Jacob, "High Accuracy Navigation and Landing System using GPS/IMU System Integration," in IEEE 1994 Position Location and Navigation Symposium, Las Vegas, NV, USA, pp. 298-305, 1994.

[33] *The Global Positioning System: A Shared National Asset*, National Research Council, Washington, D.C.: National Academy Press, 1995.

[34] *RTCM Recommended Standards for Differential Navstar GPS Service*, Version 2.1, RTCM Special Committee No. 104, January 3, 1994.

[35] Rowson, S. V., G. R. Courtneyand, and R. M. Hueschen, "Performance of Category IIIB Automatic Landings Using C/A Code Tracking Differential GPS," Navigation, Vol. 41, No. 3, pp 127-143, 1994.

[36] J. W. Spalding and L. A. Luft, "Differential GPS Integrity Monitor," in IEEE 1994 Position Location and Navigation Symposium, Las Vegas, NV, USA, pp. 225-232, 1994.

[37] H. Schneidermann and M. Nashman, "Visual processing for autonomous driving," in IEEE Workshop on Applications of Computer Vision, Palm Springs, CA, pp. 164-171, 1992.

[38] S. Shladover, et al., "Automatic Vehicle Control Developments in the PATH Program," *IEEE Trans. on Vehicular Technology*, Vol. 40, no.1, pp. 114-130, 1991.

[39] Teunissen, P. "A New Method for Fast Carrier Phase Ambiguity Estimation," *IEEE 1994 PLANS*, pp. 562-573.

[40] C. Thorpe, et al, "Toward autonomous driving: the CMU Navlab", Part 1-Perception, *IEEE Expert*, Vol. 6, pp. 31-42, 1991.

[41] Widnall, W. S. and P. A. Grundy, "Inertial Navigations System Error Models," Intermetrics Inc., TR-03-73, May 11, 1973.

[42] T. Younglove, E. Johnston, and M. Barth, "DGPS Technology for Vehicle Parameter Estimation," in International Workshop on Driving Cycles and Vehicle Data-logging, Ottawa, Canada, 1995.

[43] Zhang, et al., "An Intelligent Roadway Reference system for Vehicle Lateral Guidance/Control," in American Control Conference, San Diego, CA, pp. 281-286, 1990.

Appendix A

Appendix: Constant and Notation Definition

A.1 Notation

The notational conventions described in Table A.1 will be used throughout this report. They are based on those defined in [6].

$\mathbf{x}$	denotes the true value of x
$\hat{\mathbf{x}}$	denotes the calculated value of x
$\tilde{\mathbf{x}}$	denotes the measured value of x
$\delta\mathbf{x}$	denotes the error $x - \hat{x}$
$\mathbf{R}_{a2b}$	denotes the transformation from coordinate system a to coordinate system b
$(\mathbf{x})^a$	denotes vector x being coordinatized in frame a

Table A.1: Notation Definition

Coordinate systems will be designated by the abbreviations of Table A.2. Therefore, the rotation for a vector

a	accelerometer coordinates (non-orthogonal)
b	body coordinates
e	ECEF coordinates
g	gyro coordinates (non-orthogonal)
i	inertial coordinates
p	platform coordinates
t	tangent plane coordinates

Table A.2: Reference Frame Abbreviations

from body coordinates to tangent plane coordinates would be denoted R_{b2t}.

Table A.3 defines several variables used in this report. Great effort is placed on not using the same symbol for more than one variable, but this is not always possible.

λ	geodetic latitude (rad)
Φ	geodetic longitude (rad)
h	geodetic altitude (m)
n	north component of position (m)
e	east component of position (m)
v_N	north component of velocity (m/s)
v_E	east component of velocity (m/s)
v_D	down component of velocity (m/s)
ϕ	roll Euler angle (rad)
θ	pitch Euler angle (rad)
ψ	heading (true) Euler angle (rad)
p	angular rate about platform u axis (rad/s)
q	angular rate about platform v axis (rad/s)
r	angular rate about platform w axis (rad/s)
(f_u, f_v, f_w)	platform components of specific force
(f_N, f_E, f_D)	navigation frame components of specific force
(b_u, b_v, b_w)	accelerometer biases in platform frame
(b_p, b_q, b_r)	gyro biases in platform frame

Table A.3: Variable Definitions

A.2 Constants

The GPS satellite position calculations are very sensitive to errors in angular quantities, due to the large radius of their orbit. Table A.4 specifies the values of several constants, consistent with the WGS-84 geodetic system of coordinates, that were used in the implementation described herein.

Constant	Value	Units	Description
π	3.1415926535898		pi
ω_e	$7.2921151467 \times 10^{-5}$	rad/s	WGS-84 value of the earth rotation rate
μ	3.986005×10^{14}	$\frac{m^3}{s^2}$	WGS-84 value for Earth's universal gravitational constant
c	2.99792458×10^{8}	$\frac{m}{s}$	Speed of light
g	calculated	$\frac{m}{s^2}$	gravitational acceleration at the earth surface
F	$-4.442807633 \times 10^{-10}$	$\frac{s}{m^{.5}}$	
a	6378137.0	m	WGS-84 earth semi-major axis
b	6356752.3	m	WGS-84 earth semi-minor axis
l_1	1575.42	M Hz	L1 carrier frequency
l_2	1227.60	M Hz	L2 carrier frequency
λ_1	19.0	cm	L1 wavelength
λ_2	24.4	cm	L2 wavelength
λ_w	86.1	cm	wide lane wavelength
λ_n	10.7	cm	narrow lane wavelength

Table A.4: Important constants

Appendix B

Appendix: Platform and Experiment Photographs

This appendix contains three photographs. Figure B.1 is a photograph of the GPS antenna mounted on the instrument platform. The ultimate product would be smaller and rigidly attached to the vehicle frame. This rigid, yet movable, platform was required to allow various forms of testing. Figure B.2 shows the platform and computer equipment mounted on the 'Wipeout' ride at Castle Amusement Park. The instrument portion of the platform is enclosed in styrofoam to decrease airflow and sunlight induced temperature changes. Figure B.3 shows the location of the 'Wipeout' ride. Note the nearby metal surfaces and foilage.

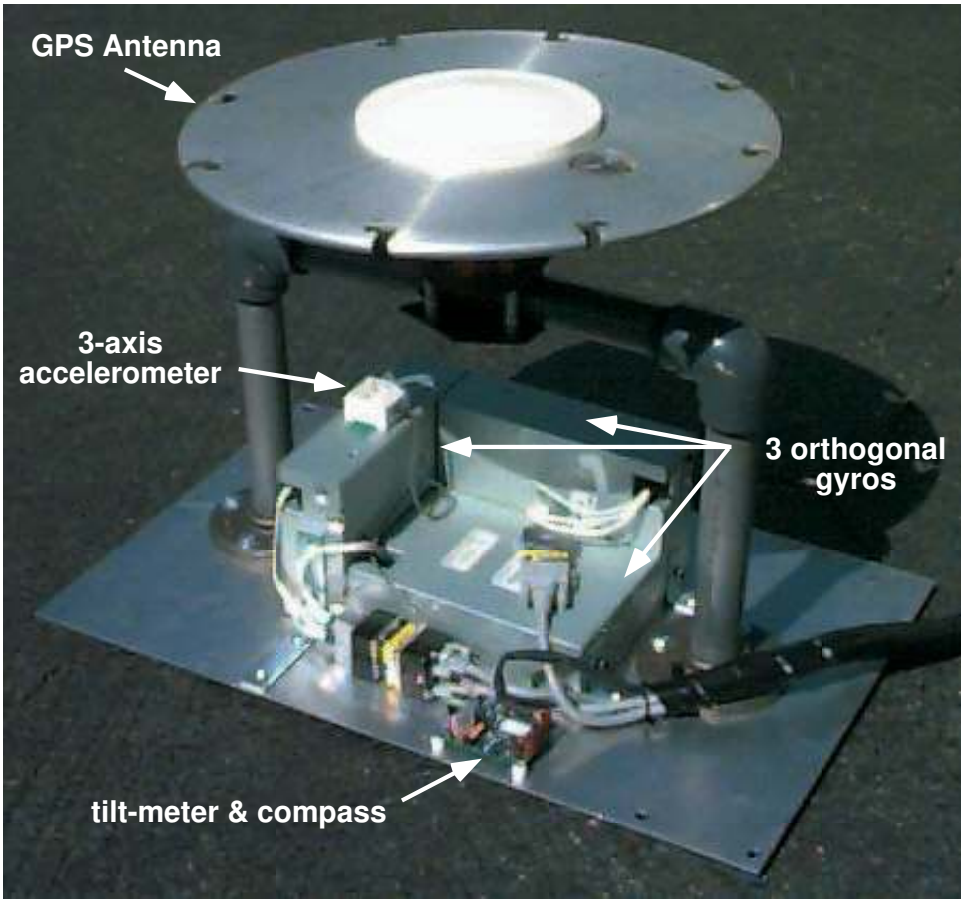

Figure B.1: GPS Antenna and Inertial Sensors Mounted on Platform

Figure B.2: GPS/INS Platform Mounted on 'Wipeout' Ride

Figure B.3: Setting of the 'Wipeout' Ride

Appendix C

Appendix: Receiver Price and Performance History

C.1 GPS Positioning Accuracy

As shown in Figure C.1, GPS accuracies have improved considerably over the operational goal of 15m. In the early 1980's carrier phase techniques were developed that gave accuracies of a few centimeters. These techniques required post processing so they were not useful for real time applications. From the mid 1980's code differential systems were producing accuracies of about 1 meter. In the early 1990's algorithm improvements and increased processing power allowed for real time carrier phase techniques. All of these techniques require differential reference stations and the accuracy is dependent on the distance between the reference station and the rover. Continuing advances in algorithms, receivers, and the GPS satellite system are still improving GPS positioning accuracy.

C.2 Receiver Cost

The cost of receivers, see Figure C.2, has declined dramatically as the price of processors (a significant part of a receiver) has decreased and as production volume has increased. Dual frequency receivers are still expensive primarily due to low production volume. As the use of two frequency receivers for high accuracy applications becomes more widespread, their cost should decrease significantly.

There have recently been a number of proposals to add a second civilian frequency (L5 or Lc) or a new military frequency (Lm), but it has been very difficult to find a suitable frequency spectrum. The utility of a second civilian frequency is becoming clear in the FAA's attempts to use GPS for Category I instrument landings. The most recent proposal by the GPS Joint Program Office [2] is a frequency partitioning in which civilians would get the +/- 4 MHz either side of the current L1 and L2 frequencies and the military would get from 4 to 12 MHz above and below the current L1 and L2 center frequencies. If this proposal is adopted dual frequency receivers should not cost more than twice the cost of a single frequency receiver because C/A code will be available for the L2 frequency.

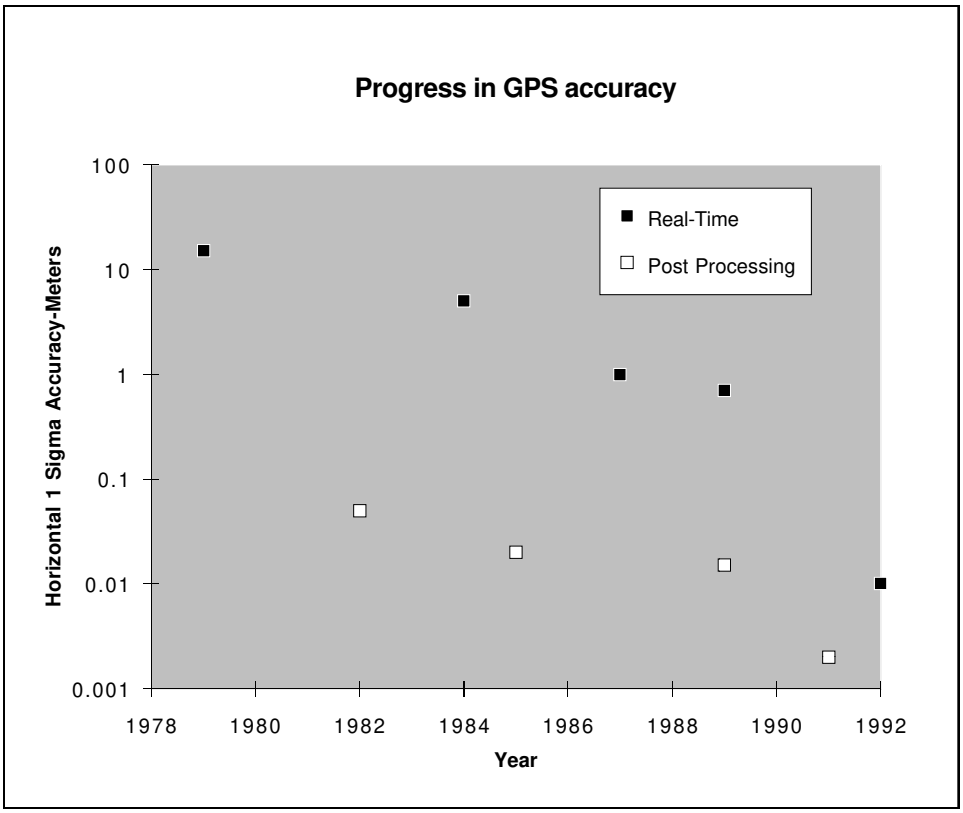

Figure C.1: GPS Standalone Position Accuracy versus Time

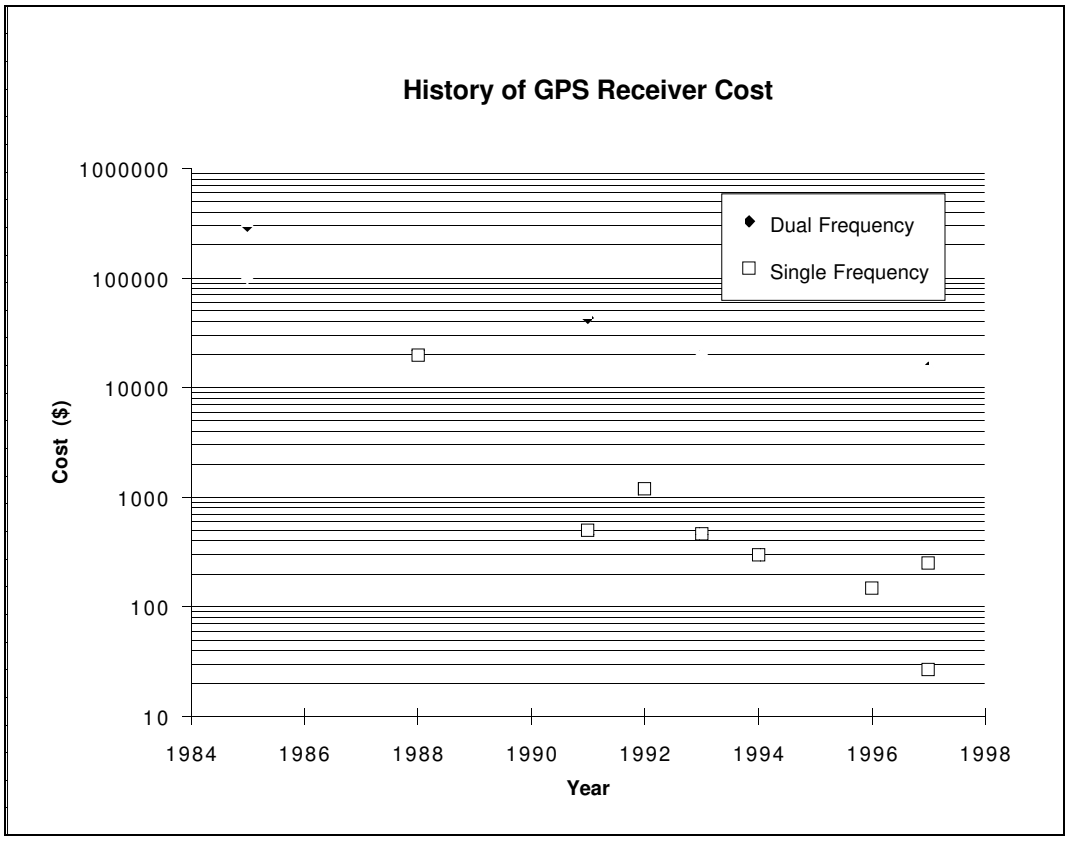

Figure C.2: GPS Receiver Cost versus Time